Semi Annual Report

Grant NAG-1-703

Research on Computational Fluid Dynamics and Turbulence

(NASA-CR-180304) RESEARCH ON COMPUTATIONAL FLUID DYNAMICS AND TURBULENCE Semiannual Report (Brown Univ.) 80 p Avail: NTIS HC A05/MF A01 CSCL 12A G3/64

N87-28346
--THRU--
N87-28348
Unclas
0094208

1) Preconditioning matrices for Chebyshev derivative operators in several space dimension.

We enclose a paper by E. Rothman explaining and summerising the problem. A joint paper with D. Funaro is being completed.

2) The Jacobi matrix technique in computational fluid dynamics.

We enclose the Ph.D. thesis of T. Sharp that was completed under this grant.

3) Chebyshev techniques for periodic problems.

We have developed Chebyshev techniques for periodic problems. These techniques give rise to differentiation matrices that have purely imaginary eigenvalues for odd number of derivatives and real and negative for even derivatives. We have demonstrated that for flows with boundary layer behaviour the periodic Chebyshev method is superior to Fourier methods.

Wai-Sun Don, a graduate student in the division, is applying those ideas to simulate flows around a circular cylinder. Dr. D. Rudi of the Computational Method Branch provides supervision for this project.

PRECONDITIONING MATRICES FOR CHEBYSHEV DERIVATIVE OPERATORS

Ernest E. Rothman

ABSTRACT:

The problem of preconditioning the matrices arising from pseudo-spectral Chebyshev approximations of first order operators is considered in both one and two dimensions. In one dimension a preconditioner represented by a full matirx which leads to preconditioned eigenvalues that are real, positive and lie between 1 and $\pi/2$, is already available. Since there are cases in which it is not computationally convenient to work with such a preconditioner, we study a large number of preconditioners which are "more sparse" (in particular three and four diagonal matrices). The eigenvalues of such preconditioned matrices are compared. In particular, the analysis is carried out for the quantity $\max|\lambda i|/\min|\lambda i|$, where λ_i are the preconditioned eigenvalues.

We apply the results to the problem of finding the steady state solution to an equation of the type $u_t = u_x + f$, where Chebyshev collocation is used for the spatial variable and time discretization is performed by the Richardson method.

In two dimensions different preconditioners are proposed for the matrix which arises from the pseudo-spectral discretization of the steady state problem in the square

$$A = \{(x,y,): -1 \leq x \leq 1, -1 \leq y \leq 1\}$$

$$U_x + U_y = f$$

$$U(x, y, 0) = U_0$$

with boundary conditions at $x = 1$ and $y = 1$. Results are given for the CPU time and the number of iterations using a Richardson iteration method for the unpreconditioned and preconditioned cases.

1. INTRODUCTION

To obtain the pseudo-spectral or collocation approximation let P_N be an interpolation operator. Let f(x) be a sufficiently smooth function defined in [-1,1] where f(x)=0 at the appropriate boundaries which yields a well-posed problem for (1.1). Then $P_N f$ is the interpolation of f at the collocation points x_j, i.e.

$$P_N f(x_j) = f(x_j) \quad \text{and} \quad P_N f \epsilon B_N. \quad j = 0,...,N$$

To obtain a Chebyshev Gauss-Lobatto pseudo-spectal approximation in the interval [-1,1] we choose $x_j = \cos j\pi/N$ (j = 0,...,N), which when $j \neq 0,N$ are the extrema of the N^{th} order Chebyshev polynomials $T_N(x) = \cos(N \cos^{-1}x)$. In order to construct the interpolant of f(x) at x, we define the polynomials

$$g_j(x) = \frac{(1-x^2)T_N'(x)(-1)^{j+1}}{\bar{c}_j N^2 (x - x_j)} \quad (j = 0,...,N)$$

$$\bar{c}_0 = \bar{c}_N = 2, \quad \bar{c}_j = 1 \quad (1 \leq j \leq N-1).$$

One can easily see that $g_j(x_k) = \delta_{jk}$.

The N^{th} degree interpolation polynomial $P_N f$ to f is given by

$$P_N f(x) = \sum_{j=0}^{N} f(x_j) g_j(x) \qquad x \epsilon \mathbb{R} \tag{1.8}$$

We must now be able to express derivatives of $P_N f$ in terms of f at the collocation points x_j. Differentiating (1.8) we obtain

$$\frac{d^n P_N f(x)}{dx^n} = \sum_{j=0}^{N} f(xj) \frac{d^n}{dx^n} g_j(x) \tag{1.9}$$

so that

$$\frac{d^n P_N f(x_k)}{dx^n} = \sum_{j=0}^{N} f(x_j) (D_n)_{kj} \tag{1.10}$$

where

$$(1.11) \qquad (D_n)_{jk} = \frac{d^n}{dx^n} g_k(x)\Big|_{x = x_j}$$

The pseudo-spectral Chebyshev derivative operator can be represented by the $N \times N$ matrix $S_n = [s_{ij}]$,

where

$$s_{jk} = \frac{\bar{c}_j (-1)^{j+k}}{\bar{c}_k (x_j - x_k)} \quad (k \neq j)$$

$$s_{jj} = \frac{-x_j}{2(1 - x_j^2)}, \quad s_{00} = \frac{2N^2 + 1}{6} = -s_{NN}$$

In particular the Chebyshev pseudo-spectral approximation for $u_t = u_x$, $u(x,0) = u_0(x)$ is given by $u_N = \sum_{k=0}^{N} u(x_j,t) g_j(x)$ and

$$\frac{\partial u_N}{\partial t}(x_j,t) = \sum_{k=0}^{N} u(x_j,t) s_{kj} .$$

2. OUTLINE OF THE PROBLEM

In the interval [-1,1] let

$$\xi_j = \cos \frac{2j-1}{2N} \pi \qquad (j = 1,2,...,N)$$

ξ_j lies between x_j and x_{j-1}

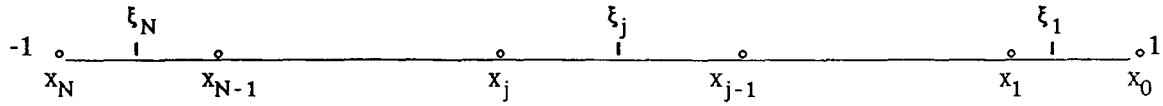

The modes x_j and ξ_j have the following properties:

$$T_N(\xi_j) = 0 \quad j = 1,...,N, \text{ and } T_N(x_i) = (-1)^i \quad i = 0,...,N$$

Then consider the pseudo-spectral Chebyshev derivative operator with homogeneous boundary conditions at x = 1. This operator can be represented by the N × N matrix $S_N = \{s_{ij}\}$, where

$$S_N = \begin{cases} \dfrac{-2N^2 + 1}{6} & \text{if } i = j = N \\ \dfrac{\bar{c}_i(-1)^{j+i}}{\bar{c}_j(x_i - x_0)} & \text{if } i \neq j \\ \dfrac{-x_j}{2(1 - x_j^2)} & \text{if } i = j = 1,...,N-1 \end{cases}$$

The matrix S_N is full. The condition number $C(S_N)$ of S_N is large. We have the following result which was obtained by Daniele Funaro.

Lemma 1-1: The condition number of S_N increases at least like N^2.

Proof: Let $\|\cdot\|$ denote the norm in $\mathfrak{L}(\mathbb{R}^N,\mathbb{R}^N)$. Then the condition number of S_N is given by

(2.1) $$c(S_N) = \|S_N\| \, \|S_N^{-1}\| .$$

It is known that $\|S_N\| \geq \rho(S_N) \geq C_1 N^2$, where $\rho(S_N)$ is the spectral radius of S_N and c_1 is a constant independent of N. On the other hand, we have

$$\|S_N^{-1}\| = \sup_{\|\vec{\varphi}\|_{\mathbb{R}^N} = 1} \|S_N^{-1}\vec{\varphi}\|_{\mathbb{R}^N}. \tag{2.2}$$

Choose $\vec{\varphi}_0 = \left[\frac{1}{\sqrt{N}},\ldots,\frac{1}{\sqrt{N}}\right]$. Then $\|\vec{\varphi}_0\|_{\mathbb{R}^N} = 1$ and $(S_N^{-1}\vec{\varphi}_0)_j = \frac{1}{\sqrt{N}}(x_j - 1)$, for $j = 1,\ldots,N$. Furthermore,

$$\|S_N^{-1}\vec{\varphi}_0\|_{\mathbb{R}^N} = \frac{1}{\pi}\sum_{j=1}^{N}(x_j - 1)^2\frac{\pi}{N} \geq \frac{1}{\pi}\int_{-1}^{1}(x - 1)^2\,\omega dx = c_2 \tag{2.3}$$

where c_2 does not depend on N.

This implies $\|S_N^{-1}\| \geq \|S_0^{-1}\vec{\varphi}_0\|_{\mathbb{R}^N} \geq c_2$. Finally, using (2.1), we get $C(S_N) \geq C_3 N^2$. This proves the claim.

Although the condition number is particularly meaningful for numerical applications, its determination is generally very difficult. Another quantity which is meaningful for practical application is $\sigma(M) = \max_i|\lambda_i|/\min_i|\lambda_i|$ where M is an $N \times N$ matrix and λ_i $i = 1,\ldots,N$ are its eigenvalues. It can be shown empirically that $\sigma(S_N)$ behaves like N.

We are interested in finding a "preconditioner" for S_N. In particular we are concerned with finding a matrix R_N such that the quantitity $\sigma(R_N^{-1}S_N)$ is small. In general this does not imply that the corresponding condition number will be small (so the word "preconditioner" is not correct).

In [DF] S_N is preconditioned by $R_N = Z_N D_N$ where the $N \times N$ matrix $D_N = \{d_{ij}\}$ is defined by

$$d_{ii} = -1/(x_{i-1} - x_i) \qquad i = 1,\ldots,N$$

$$d_{ii-1} = 1/(x_{i-1} - x_i) \qquad i = 2,\ldots N$$

$$d_{ij} = 0 \qquad \text{otherwise}$$

Hence D is the upwind finite differences matrix relative to the grid x_i. $Z_N: P_{N-1} \to P_{N-1}$ is the operator which maps the values of a polynomial in P_{N-1} at the staggered grid points $\{\xi_1,...,\xi_N\}$ into the values at the mesh points $\{x_1,...,x_N\}$.

Preconditioning by $Z_N D_N$ results in preconditioned eigenvalues that are real, positive and lie between 1 and $\pi/2$. The ratio $\sigma(D_N^{-1} Z_N^{-1} S_N)$ is bounded by $\pi/2$ (see [DF]). This is particularly interesting when the solution of the system

$$S_n u + f = 0 \tag{2.4}$$

has to be found. If an iterative method is used, iterating $M_N = (Z_N D_N)^{-1} S_N$ instead of S_N results in convergence in a few iterations. In the end of the computation the system $(Z_N D_N)u + f = 0$ has to be solved. So we require that the matrix $R_N = Z_N D_N$ can be inverted easily. Although Z is a full matrix, it can be inverted very inexpensively in N log N operations. Thus the matrix $R_N = Z_N D_N$ can be inverted very inexpensively. Nevertheless there are cases in which it is not computationally convenient to work with a full preconditioner.

In particular when using an implicit method to find the solution at time $T > 0$ of the equation

$$\begin{aligned} u_t &= S_N u + f, \\ u(x,0) &= u_0(x), \\ u(1,t) &= 0 \quad 0 \leq t \leq T. \end{aligned} \tag{2.5}$$

If the implicit Euler method is used, iterates of the matrix $(I + \Delta t S_N)$ are considered. A good preconditioner for this matrix turns out to be the matrix $(I + \Delta t Z_N D_N)$. Unfortunately, due to the fact that Z_N is a full matrix, $(I + \Delta t Z_N D_N)$ cannot be inverted inexpensively. In this work we shall present a large number of preconditioners which can be applied to the situations illustrated above.

3. ANALYSIS IN ONE DIMENSION

In order to have the matrix $I + \Delta t\, Z_N D_N$ which can be easily inverted we substitute Z_N by some suitable matrix which has a simpler form and which has to be regarded as an approximation of the operator related to Z_N.

The first idea is the following. Take $\tilde{Z}_N = \{\tilde{z}_{ij}\}$ such that

(3.1)
$$\tilde{z}_{ii} = .5$$
$$\tilde{z}_{ii+1} = .5$$
$$\tilde{z}_{NN} = 1.$$

Then $\tilde{Z}_N D_N$ is a tridiagonal matrix so tha $I + \Delta t\, \tilde{Z}_N D_N$ is also a tridiagonal matrix. It can be shown that the eigenvalues of $M_N = (\tilde{Z}_N D_N)^{-1} S_N$ take the following form.

$$\lambda_k = k \sum_{j=0}^{k-1} x_j \qquad k = 1,...,N$$

Thus, the eigenvalues of the preconditioned matrix are real and positive. Hence we have $\sigma(M_N) = N$. The choice of $\tilde{Z}_N$ as in (3.1) corresponds to shifting the values from the staggered mesh to the initial mesh by averaging the two neighbour values. Instead of this we can choose $\tilde{Z}_N = \{\tilde{Z}_{ij}\}$ corresponding to interpolation by first order polynomials. This leads to the following definition of the matrix $\tilde{Z}_N = \{\tilde{Z}_{ij}\}$

(3.2)
$$z_{ii} = \frac{x_i - \xi_{i+1}}{\xi_i - \xi_{i+1}} \qquad i = 1,...,N-1$$
$$z_{ii+1} = \frac{x_i - \xi_i}{\xi_{i+1} - \xi_i} \qquad i = 1,...,N-1$$

We found emperically, that the eigenvalues of the preconditioned matrix are still real and positive, but the quantity $\sigma(M_N)$ is now worse than that of the previous case.

Another simple preconditioner which this time is not of the form $Z_N D_N$ is defined

by $R_N = \{r_{ij}\}$ where

$$
\begin{aligned}
& r_{ii} = 0 && i = 1,\ldots,N-1 \\
& r_{NN} = 1/(x_{N-1} - x_N) && \\
(3.3) \qquad & r_{i,i+1} = 1/(x_{i-1} - x_{i+1}) && i = 1,\ldots,N-1 \\
& r_{i,i-1} = 1/(x_{i-1} - x_{i+1}) && i = 2,\ldots,N-1 \\
& r_{N-1,N} = 1/(x_{N-1} - x_N) &&
\end{aligned}
$$

In this case we still get real and positive preconditioned eigenvalues. Namely, they take the form:

$$\left\{\lambda_k = \frac{k \sin \pi/N}{\sqrt{1 - x_k^2}} \quad k = 1,\ldots,N-1\right\} \cup \{\lambda_N\},$$

where λ_N is approximately equal to 2.46. We have $\sigma(M_N) = N-1$. This is the best we tested using tridiagonal preconditioners. Up to now the improvements are poor so we have to consider better approximations of the matrix Z_N.

We consider an approximation of the operator related to Z_N by interpolation with a polynomial of degree 2. One possible choice is the following: $\tilde{Z} = \{\tilde{z}_{ij}\}$ where

$$
\left\{
\begin{aligned}
& \hat{z}_{11} = (x_1 = \xi_2)/(\xi_1 - \xi_2) \\
& \hat{z}_{12} = (x_1 - \xi_1)/(\xi_2 - \xi_1) \\
& \hat{z}_{i,i-1} = (x_i - \xi_i)(x_i - \xi_{i+1})/((\xi_{i-1} - \xi_i)(\xi_{i-1} - \xi_{i+1})) && i = 2,\ldots,N-1 \\
(3.4) \qquad & \hat{z}_{ii} = (x_i - \xi_{i-1})(x_i - \xi_{i+1})/((\xi_i - \xi_{i-1})(\xi_i - \xi_{i+1})) && i = 2,\ldots,N-1 \\
& \hat{z}_{i,i+1} = (x_i - \xi_{i-1})(x_i - \xi_i)/((\xi_{i+1} - \xi_{i-1})(\xi_{i+1} - \xi_i)) && i = 2,\ldots,N-1 \\
& \hat{z}_{N,N-1} = (x_N - \xi_N)/(\xi_{N-1} - \xi_N) \\
& \hat{z}_{NN} = (x_N - \xi_{N-1})/(\xi_N - \xi_{N-1})
\end{aligned}
\right.
$$

Now $\hat{Z}$ is a three-diagonal matrix, hence $\hat{Z}D$ is a four-diagonal matrix. The numerical experiments performed up to N = 32 give the following results. The eigenvalues λ of

$M_N = \hat{(Z_N D_N)^{-1} S_N}$ are in general complex. The have positive real part greater than .98. Most of them are concentrated at 1. Figure 3.1 shows the behavior of the λ's for N = 12 and N = 20.

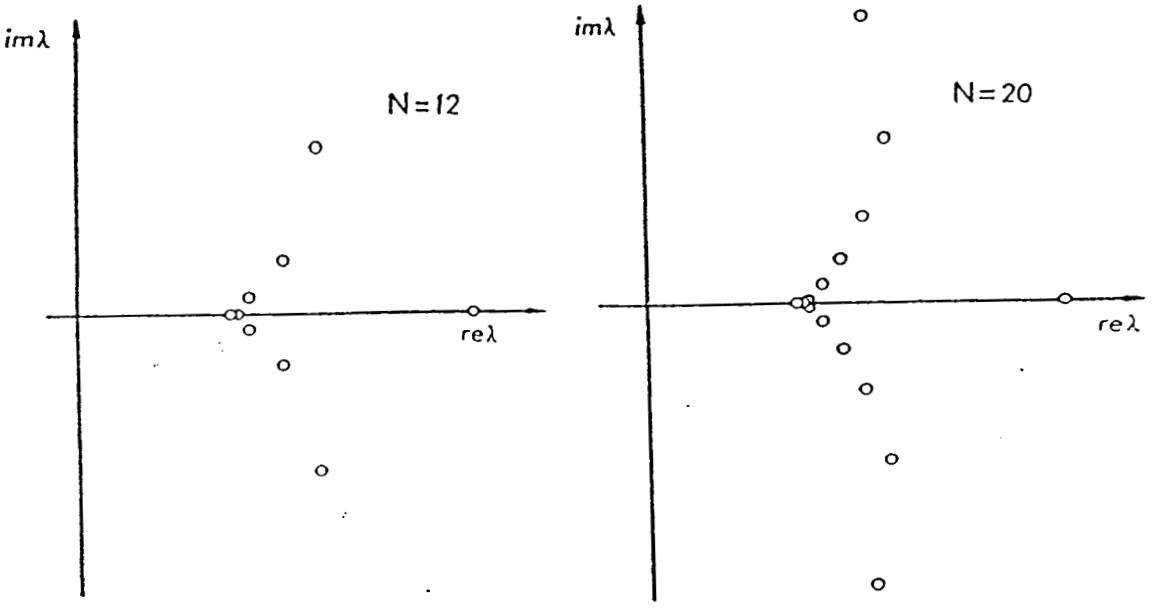

Figure 3.1 - Location of the preconditioned eigenvalues in the complex plane.

The corresponding $\sigma(M_N)$ is represented in Table 3.1 for various N. This time $\sigma(M_N)$ is bounded with respect to N.

N	$\sigma(M_N)$
8	2.602
16	2.724
24	2.758
32	2.770

Table 3.1 - Case of Four-diagonal preconditioner

Other possibilities for the tridiagonal matrix $\hat{Z}$ were tested. For example one possible choice, analogous to that of the matrix in (3.1), is to take $\hat{Z}_N = \{\hat{z}_{ij}\}$ such that

$$\begin{aligned} \hat{z}_{i,i-1} &= -1/8 \\ \hat{z}_{ii} &= 3/4 \\ \hat{z}_{i,i+1} &= 3/8 \end{aligned} \tag{3.5}$$

Among all the experiments, the matrix proposed in (3.4) gives the best results. Five-diagonal preconditioners were tested, through interpolation by third degree polynomials. The results do not imporve those corresponding to Table 3.1.

Now, if the system of linear equations (1.5) is solved, for example, by the implicit Richardson method, we are concerned with $\sigma(M_N)$, where $M_N = (I + \Delta t\, \hat{Z}_N D_N)^{-1}(I + \Delta t\, S_N)$ and $\hat{Z}_N$ is the matrix in (3.4). The graph of $\sigma(M_N)$ versus Δt is reported in Figure 2.2 for some values of N. So, in addition to the fast convergence of the iterative scheme, the preconditioning matrix can be inverted efficiently.

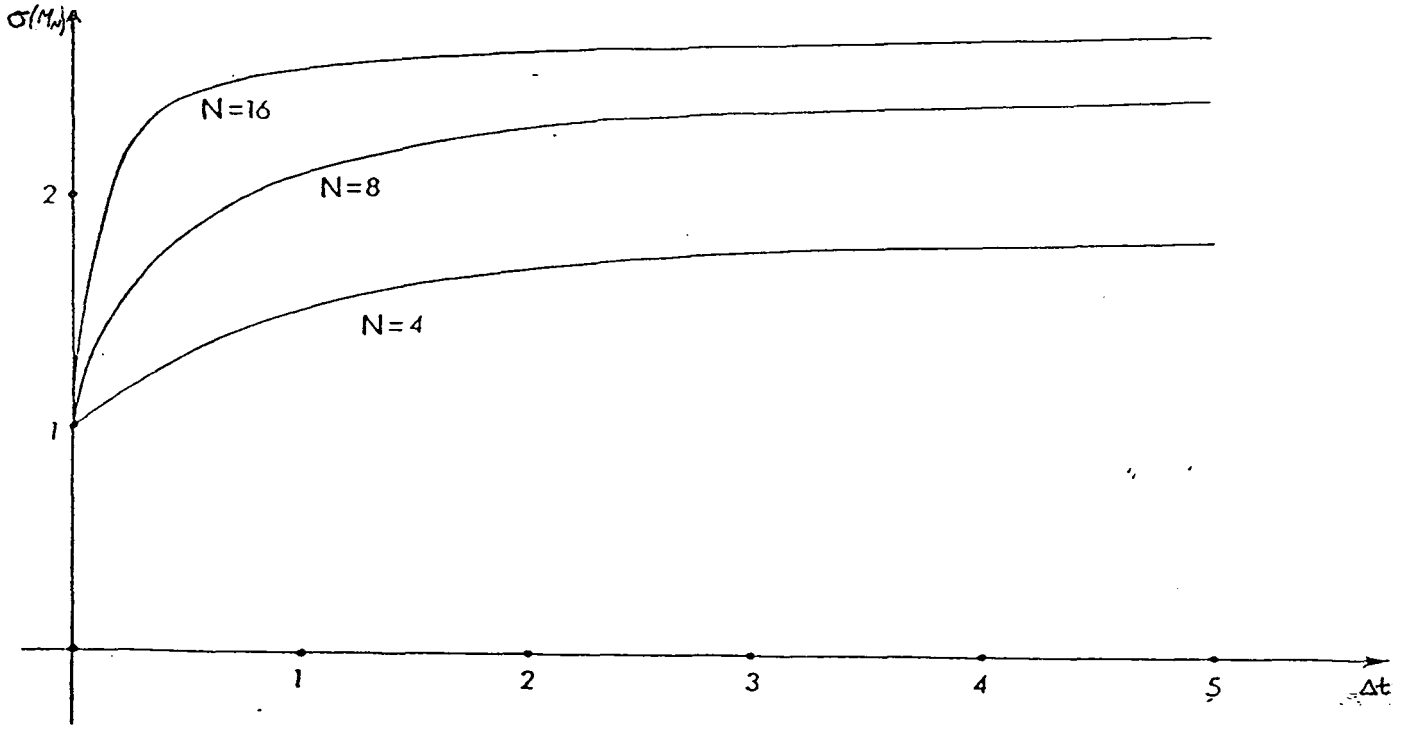

Figure 3.2

Now, if the steady state solution of problem (2.5) has to be found (which corresponds to the solution of problem (2.4), the explicit Richardson method can be used. This leads to the iterative scheme

$$u^{n+1} = (I + \Delta t S_N)u^n \ , \ n \in N \tag{3.6}$$

If λ denotes the general eigenvalue of S_N, the scheme is stable provided we choose Δt such that

$$0 < \Delta t < \inf_{\lambda}\left[\frac{-2Re\lambda}{|\lambda|^2} \right]. \tag{3.7}$$

Within the stability region we have $\rho(I + \Delta t S_N) < 1$ where ρ denotes the spectral radius.

In order to speed up the convergence we experimentally find Δt^* such that $\rho(I + \Delta t^* S_N)$ attains its minimum inside the interval of stability. In general Δt^* is not available. We use it here only to compare preconditioners. The same experiments are made for the preconditioned schemes, i.e.:

$$u^{n+1} = (I + \Delta t Z_N D_N)^{-1}(I + \Delta t S_N)u^n \tag{3.8}$$

$$u^{n+1} = (I + \Delta t \hat{Z}_N D_N)^{-1}(I + \Delta t S_N)u^n \tag{3.9}$$

where Z_N and $\hat{Z}_N$ are respectively, the full matrix proposed in [DF] and the tridiagonal matrix given by (3.4).

Both the schemes (3.8) and (3.9) converge to the same solution of (3.6). The results of these experiments are reported in Tables 3-2, 3-3, and 3-4

N	Maximum Δt for Stability	Δt^*	ρ Corresponding to Δt^*
8	.05461	.02724	.9817
16	.01836	.009120	.9919
24	.009232	.005244	.9939
32	.005138	.002521	.9966

Table 3-2 Minimum spectral radius of the unpreconditioned amplification matrix

N	Maximum Δt for Stability	Δt^*	ρ Corresponding to Δt^*
8	1.281	.7810	.2190
16	1.275	.7787	.2213
24	1.274	.7783	.2217
32	1.274	.7782	.2218

Table 3-3 Minimum spectral radius of the preconditioned matrix: case of Z_N.

N	Maximum Δt for Stability	Δt^*	ρ Corresponding to Δt^*
8	.7685	.5552	.4448
16	.6381	.3190	.7112
24	.4258	.2129	.8465
32	.3210	.1605	.9043

Table 3-4 Minimum spectral spectral radius of the preconditioned matrix: case of $\hat{Z}_N$

We also considered the second order Runge-Kutta scheme. This leads to the iterative scheme

$$u^{n+1} = (I + \Delta t S_N + \frac{\Delta t^2}{2} S_N^2)u^n \quad , \quad n \in N \tag{3.10}$$

In this case the stability restriction on Δt is given by

$$\Delta t^3 |\lambda|^4 + 4\,\Delta t^2 (Re\lambda)|\lambda|^2 + 8\Delta t (Re\lambda)^2 + 8Re\lambda < 0. \tag{3.11}$$

for all eigenvalues, λ, of S_N. We obtained results that were qualitatively analogous to that of Tables 3-2, 3-3, and 3-4.

4. ANALYSIS IN TWO DIMENSIONS

In two dimensions we will consider the following steady state problem on the square $A = \{(x,y): -1 \leq x \leq 1, -1 \leq y \leq 1\}$ with homogeneous boundary conditions at $x = 1$, and $y = 1$.

(4.1)
$$u_x + u_y = f$$
$$u(x,y,0) = u_0 \qquad (x,y)\epsilon A$$
$$u(1,y,t) = u(x,1,t) = 0. \qquad t \geq 0$$

The essential idea in obtaining a pseudo-spectral approximation to (4.1) is the same as it was in 1-dimension. That is, to approximate spacial derivatives by constructing a global interpolant through discrete points. To obtain the Chebyshev pseudo-spectral approximation we take as these points $x_j = y_j = \cos \pi j/N$ for $j = 1,2,...,N$. This means that we must interpolate at the N^2 points (x_i,y_j) for $i,j = 1,2,...,N$. Consequently, the Chebyshev derivative operator for this problem can be represented by the $N^2 \times N^2$ matrix $S_N^{(2)} + P^t S_N^{(2)} P$, where $S_N^{(2)}$ is a block diagonal matrix whose blocks are each equal to S_N, and P is a permutation matrix. If one orders the N^2 points (x_i,y_j) by rows then $S_N^{(2)}$ corresponds to the derivative in the x-direction and P is constructed so that $P^t S_N^{(2)} P$ corresponds to the derivative in the y-direction. Without preconditioning $S_N^{(2)} + P^t S_N^{(2)} P$ is ill-conditioned.

As we saw in section 3 ZD is a good preconditioner for S_N. Thus, a natural approach to finding a preconditioner for $S_N^{(2)} + P^t S_N^{(2)} P$ is to try $Z^{(2)} D^{(2)} + P^t Z^{(2)} D^{(2)} P$, where $Z^{(2)}$ and $D^{(2)}$ are $N^2 \times N^2$ block diagonal matrices whose blocks are the $N \times N$ matrices Z and D, respectively.

To analyze the behavior of the eigenvalues of the preconditioning matrix, we define λ as the generic eigenvalue of the preconditioned matrix, $\rho_N = \max_i |\lambda_i| / \min_i |\lambda_i| (i = 1,2,...N^2)$, σ_N is the maximum σ such that $\mathrm{Re}\,\lambda \geq \sigma$, and r_N is the minimum r such that $|\lambda - 1| \leq r$. In particular, r_N and σ_N give us an idea of the location of the eigenvalues. (See figure 4-1 below.)

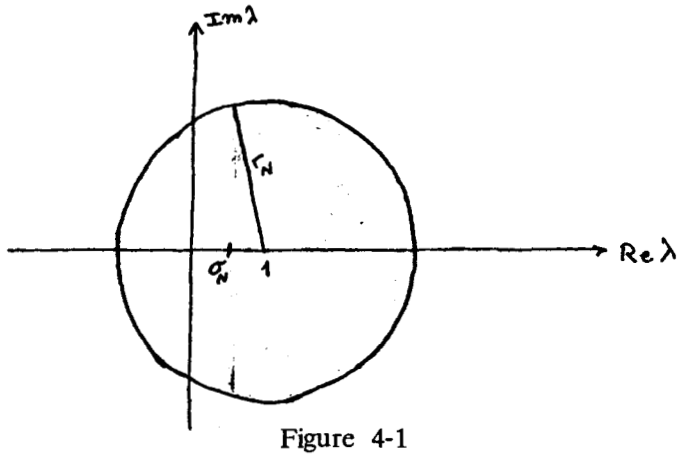

Figure 4-1

Numerical experiments performed for N = 4,6,8 are summarized in Table 4-1

N	ρ_N	r_N	σ_N
4	1.530	.530	1.000
6	1.552	.589	1.000
8	1.560	.622	1.000

Table 4-1

Although the eigenvalues of this preconditioned matrix, $(Z^{(2)}D^{(2)} + P^tZ^{(2)}D^{(2)}P)^{-1}(S_N^{(2)} + P^t S_N^{(2)}P)$, are well behaved the matrix is full and thus difficult to invert. Another approach to constructing a preconditioner is to substitute in $Z^{(2)}D^{(2)} + P^t Z^{(2)}D^{(2)}P$ the tridiagonal matrix $\hat{Z}$ defined by (2.4) in place of Z. We will denote this new $N^2 \times N^{(2)}$ matrix by $\hat{Z}^{(2)}D^{(2)} + P^t \hat{Z}^{(2)}D^{(2)}P$. This matrix represents a finite difference scheme depending on seven points as illustrated by the stencil in Figure 4-2.

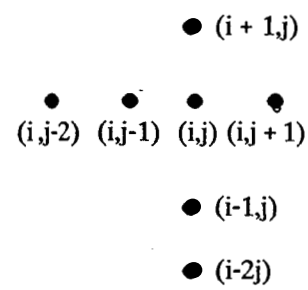

Figure 4-2

Results similar to those presented in Table 4-1 are prsented in Table 4-2 for $Z^{(2)}D^{(2)} + P^t Z^{(2)}D^{(2)}P$.

N	ρ_N	r_N	σ_N
4	2.206	.980	.897
6	5.026	1.453	.488
8	8.494	1.602	.306

Table 4-2

Although ρ_N corresponding to $\hat{Z}^{(2)}D^{(2)} + P^t \hat{Z}^{(2)}D^{(2)}P$ increases more quickly than ρ_N corresponding to $Z^{(2)}D^{(2)} + P^tZ^{(2)}D^{(2)}P$, the matrix can be inverted more efficiently. This is because $\hat{Z}^{(2)}D^{(2)} + P^t \hat{Z}^{(2)}D^{(2)}P$ is a banded matrix (with N lower codiagonals and 2N upper codiagonals).

Another preconditioner that we considered was of the form

$$Z^{(2)}P^tZ^{(2)}P(D^{(2)} + P^tD^{(2)}P).$$

As in the 1-dimensional case, if the steady-state solution is to be found, the explicit Richardson method can be used. We experimentally find Δt^* such that $\rho(I + \Delta t^* W_N)$ attains its minimum inside the region of stability. The same experiments are made for the preconditioned matrices. The results of the experiments are reported in Tables 3-3, 3-4, and 3-5.

N	Maximum Δt for Stability	Δt^*	ρ Corresponding to Δt^*
4	.1509563	.07547812	.9248009
6	.05228855	.02614427	.9715761
8	.0273053	.01365251	.9817108
10	.01944351	.009721750	.9810511

Table 4-3 Minimum spectral radius of the unpreconditioned amplification matrix

N	Maximum Δt for Stability	Δt^*	ρ Corresponding to Δt^*
4	.9879928	.7172827	.6693591
6	.9094622	.6584506	.8027519
8	.7200746	.4954113	.8715243
10	.6038381	.3623029	.8995660

Table 4-4 Minimum spectral radius of the preconditioned matrix: Case of $Z_N P^t Z_N P(D_N + P^t D_N P)$

N	Maxiumum Δt for Stability	Δt^*	ρ Corresponding to Δt^*
4	1.009613	.6946138	.3763489
6	.815170	.6798409	.6681257
8	.7685055	.6870439	37895085

Table 4-5 Minimum spectral radius of the preconditioned matrix:

Case of $\hat{Z}_N D_N + P^t \hat{Z}_N D_N P$

We also considered the second order Runge-Kutta scheme, and we obtained results that were qualitatively analogous to those of Tables 4-3, 4-4, and 4-5.

We applied the Richardson schemes in the unpreconditioned version and in the preconditioned versions using the preconditioners $\hat{Z}_N D_N + P^t \hat{Z}_N D_N P$ and $Z_N P^t Z_N P(D_N + P^t D_N P)$, to find the solution of the model problem

$$u_t = u_x + u_y - \alpha\sin(\alpha(x+1)) + \alpha\sin(\alpha(y+1)$$

$$u(x,y,0) = \sin(y-1)\sin(x-1)$$

$$u(-1,y,t) = u(x,-1,t) = 0$$

of the type in (4.1). We used the optimal Δt^* listed in tables 4-3, 4-4, and 4-5. Using the L_2 norm we considered the scheme to converge when the exact error stabilized. We also calculated global CPU times. The experiments were performed on the IBM 3081 and the results are reported in Tables 4-6,4-7, and 4-8.

N	No. of Iteration for Convergence	Error	CPU Time for Convergence (in seconds)
4	122	$.12405 \times 10^{-1}$	.21
6	400	$.104182 \times 10^{-3}$	1.33
8	900	$.47112 \times 10^{-6}$	5.82

Table 4-6 Unpreconditional Euler

N	No. of Interation for Convergence	Error	CPU Time for Convergence	CPU Time for Construction of Preconditioner and Finding LU Decomposition of Preconditioner
4	11	$.1246626 \times 10^{-1}$	.03	.00
6	34	$.10400 \times 10^{-3}$	.26	.04
8	69	$.4709596 \times 10^{-6}$	1.17	.11

Table 4-7 Preconditioned Richardson Case of $\hat{Z}_N D + P^t \hat{Z}_N DP$

N	No. of Interations for Convergence	Error	CPU Time for Convergence	CPU Time for Construction of Precondtioner and Finding LU Decomposition of Preconditioner
4	32	$.12468 \times 10^{-1}$	.09	.00
6	173	$.104255 \times 10^{-3}$	1.10	.00
8	263	$.4709613 \times 10^{-6}$	3.31	.00

Table 4-8 Precondition Richardson Case of $Z_N P^t Z_N P(D + P^t DP)$.

[DF] D. Funaro, "A preconditioning matrix for the Chebyshev differencing operator", Istituto Di Analisi Numerica del Consiglio Nazionale Delle Ricerche Corso C. Alberto, 5-27100 PAVIA (Italy) N. 509.

The Jacobi Matrix Technique in Computational Fluid Dynamics

by

H. Thomas Sharp

S.B., Physics, Massachusetts Institute of Technology, 1981

S.B., Mathematics, Masschusetts Institute of Technology, 1981

S.M., Aero. & Astro., Massachusetts Institute of Technology, 1983

M.Sc., Applied Mathematics, Brown University, 1985

Thesis

Submitted in partial fulfillment of the requirements for the
Degree of Doctor of Philosophy in the Division of
Applied Mathematics at Brown University

May 1988

This dissertation by H. Thomas Sharp

is accepted in its present form by the Division of

Applied Mathematics as satisifying

dissertation requirement for the degree of Doctor of Philosophy

Date_____ _____

Lawrence Sirovich

Recommended to the Graduate Council

Date_____ _____

Frederic E. Bisshopp

Date_____ _____

David Gottlieb

Approved by the Graduate Council

Date_____ _____

VITA

H. Thomas Sharp was born on [redacted] in [redacted]. He earned undergraduate degrees in physics and mathematics from MIT in 1981. While an undergraduate, he learned to fly and received his pilot's license in 1981. Wanting to learn more about aerodynamics, he stayed at MIT and studied computational aerodynamics in the Department of Aeronautics and Astronautics receiving a Master's degree in 1983. In the fall of 1983 he entered Brown University to study fluid dynamics in the Division of Applied Mathematics and received a Master's degree in 1985. Upon his graduation from Brown in the summer of 1987 he started working as an aerodynamicist for Lockheed-California Co..

Acknowledgements

It is with great pleasure that the author wishes to express his sincere appreciation and thanks to the following people:

Professor Lawrence Sirovich not only for suggesting the topic and providing the guidance throughout the course of this work, but also for his patience and understanding during my stay at Brown.

Professors Frederic Bisshopp and David Gottlieb for evaluating this manuscript and for their lucid explanations of and help with understanding computational fluid dynamics.

Ms. Andria Durk and Ms. Madeline Brewster for typing the seemingly endless revisions of this dissertation.

Most of all I would like to thank my parents. Their encouragement and assistance made this degree possible.

CONTENTS

INTRODUCTION

Flow past a body is, in general, specified by a variety of parameters such as thickness, angle of attack, camber, Mach number etc. A particular flow is, therefore, characterized by a single point in the corresponding parameter space. Conversely, the numerical calculation of a particular flow field yields information at just one point of the parameter space. However, the nature of a continuous range of nearby flow fields is of fundamental significance in the design and performance of aircraft. To treat this generally, one can consider the variational equations (which are linear) obtained by differentiating the exact equations with respect to each of the relevant parameters. The resulting matrix of derivatives of flow quantities is referred to as the Jacobi matrix.

The subsequent procedure is, in principle, straightforward. One integrates the nonlinear governing equations -- which results in the determination of just one point in parameter space -- and simultaneously the variational equations governing the Jacobi matrix. The last is then used to describe the neighborhood of the already determined point of the parameter space. A method is presented herein which allows efficient generation of solutions in the neighborhood of a base solution. Since the variational equations are linear, the additional computational time required for their integration is modest.

We have applied the Jacobi matrix technique to the direct calculation of inviscid supersonic flow about

- o two dimensional airfoils of varying thickness, angle of attack and camber
- o axisymmetric bodies of varying thickness and taper

and the design (inverse) calculation of inviscid supersonic flow past

- o airfoils described by a given family of pressure distributions
- o axisymmetric bodies described by a given family of pressure distributions.

Also we applied the method to subsonic potential flow about two dimensional

airfoils by modifying Jameson's FLO36.

Results of our calculations show that the Jacobi method allows for the efficient and accurate generation of parametric solutions in the neighborhood of a known solution. In general terms, we consider a system of nonlinear partial differential equations

$$\underline{F}\ (\underline{u}\,(\underline{x};\underline{\epsilon}), \underline{x};\underline{\epsilon}) = 0 \tag{I.1}$$

in the flow variables $\underline{u}$, dependent variables $\underline{x}$, and parameters $\underline{\epsilon}$. For purposes of exposition we regard $\underline{u}(\underline{x};\underline{\epsilon})$ as known and seek the solution at a neighboring point in parameter space. The parametrically differentiated dependent variables are governed by the equations obtained by differentiating (1), viz.

$$\frac{d}{d\epsilon_k} F_i\,(\,\underline{u},\underline{x};\underline{\epsilon}\,) = \frac{\partial Fi}{\partial u_j}\,\frac{\partial u_j}{\partial \epsilon_k} + \frac{\partial Fi}{\partial \epsilon_k} = 0 \tag{I.2}$$

The, in general, non-square matrix $\frac{\partial u_i}{\partial \epsilon_k}$ is known as the Jacobi matrix and the above procedure provides a linear system of equations governing the Jacobi matrix. The term $\partial F_i/\partial u_j$ actually represents an operator, the details of which are best left to the individual cases. If $\underline{u}^0 = \underline{u}(\underline{x};\underline{\epsilon}_0)$ represents a known solution of the flow then any neighboring flow at some fixed point $\underline{x}$ is determined by

$$\underline{u}\,(\underline{x};\underline{\epsilon}) \approx \underline{u}^0 + \frac{\partial \underline{u}^0}{\partial \underline{\epsilon}_k}(\underline{\epsilon}_k - \underline{\epsilon}_0) \tag{I.3}$$

In what follows we will be somewhat loose in not distinguishing between the two sides of (I.3). A basic difficulty with what has been just said, in particular to the use of (I.3), is the fact that the conditions on the problem occur at locations which vary with $\underline{\epsilon}$. Specifically, both the boundary locations (and shock locations) may vary with changes in the parameters $\underline{\epsilon}$. We first present a method that avoids the difficulties implicit in such spatial variations with $\underline{\epsilon}$, and later treat directly the formulation implicit in (I.1-3).

Chapter I

The Jacobi Matrix Technique and It's Application to Two-Dimensional Supersonic Flow

The White Rabbit put on his spectacles. "Where shall I begin, please your Majesty?" he asked.

"Begin at the beginning," the King said, very gravely, "and go on till you come to the end: then stop."

- Alice's Adventures in Wonderland
Lewis Carroll

APPLICATION TO 2D SUPERSONIC FLOW

To illustrate this method we consider steady, inviscid, supersonic flows past two dimensional airfoils. For this purpose and in order to be specific, consider a family of profiles depending on three parameters (thickness, camber, and angle of attack). For completeness, we summarize the methods used in solving such flows [1], [2]. The equations are written in characteristic form as follows:

$$s_\beta = 0 \tag{1.1}$$

$$(\theta + P(\mu))_\alpha = \frac{\sin 2\mu}{2\gamma} s'(\alpha) \tag{1.2}$$

$$(\theta - P(\mu))_\beta = (1 - \tan\theta \tan\mu) \frac{x_\beta}{x_\alpha} \theta_\alpha \tag{1.3}$$

Here the coordinates (α,β) correspond to the streamlines, α = constant, and the C^+ characteristics, β = constant (Figure 1). θ is the flow deflection angle, μ is the Mach angle and s is the entropy. $P(\mu)$ is the Prandtl function given by

$$P(\mu) = \lambda^{1/2} \tan^{-1} (\lambda^{-1/2} \tan\mu) - \mu \ , \ \lambda = (\gamma+1)/(\gamma-1) \ . \tag{1.4}$$

An advantage to solving the above characteristic form of the equations is that it generates a body fit, shock fit coordinate system. We mention in passing that since the equations are exact, they are valid in the hypersonic flow regime so long as such real gas effects as disassociation and ionization can be ignored.

The physical coordinates x,y satisfy the relations [1], [2]

$$y_\alpha = x_\alpha \tan(\theta+\mu), \qquad y_\beta = x_\beta \tan\theta \tag{1.5}$$

The transformation to (α,β) coordinates leaves open two arbitrary functions and these are fixed so that the shock is along $\alpha = \beta$ and the airfoil is positioned along the line $\alpha = 0$ (Figure 2). Appropriate boundary conditions at the body are

$$x((0,\beta) = \beta, \quad y(0,\beta) = f(\beta,\underline{\epsilon}), \quad \theta(0,\beta) = \tan^{-1}(f_\beta(\beta,\underline{\epsilon})). \tag{1.6}$$

The Rankine-Hugoniot conditions govern the jumps in θ, μ and s at the shock. Written in terms of the shock angle η, they are given by

$$\tan\theta = \frac{1}{\tan\eta} \frac{(M^2 - 1)\tan^2\eta - 1}{(1+\frac{\gamma+1}{2}M^2) + (1+\frac{\gamma-1}{2}M^2)\tan^2\eta} \tag{1.7}$$

$$\sin^2\mu = \frac{0.2(1+\frac{7}{6}w)(1+\frac{1}{6}w)}{(1+w)(1+0.2M^2) - (1+\frac{7}{6}w)(1+\frac{1}{6}w)} \tag{1.8}$$

$$s = 2.5 \ln(1+\frac{7}{6}w) + 3.5 \ln(1+\frac{1}{6}w) - 3.5 \ln(1+w) \tag{1.9}$$

where

$$w = M^2 \sin^2\eta - 1 \tag{1.10}$$

The shock angle is related to the coordinates as follows

$$\tan\eta = dy/dx \Big|_{shock} = \frac{y_\alpha + y_\beta}{x_\alpha + x_\beta}\Big|_{shock} \tag{1.11}$$

In the above we have assumed a perfect gas with constant specific heats and hence that

$$p = \rho^\gamma \exp[(\gamma - 1)s] \tag{1.12}$$

It should be noted that this formulation eliminates the difficulty mentioned in the Introduction. Namely, by using the (α,β) - coordinate system, a quantity such as

$$\frac{\partial p}{\partial \underline{\epsilon}}(\alpha, \beta; \underline{\epsilon})$$

signifies the variation with $\underline{\epsilon}$ at fixed α and β. In particular it gives the variation of pressure say fixed at the body, $\alpha = 0$, or at the shock, $\alpha = \beta$. This makes the integration of the differential equations significantly simpler.

VARIATIONAL EQUATIONS

We are interested in solutions to these equations at points near a known solution. To pursue this we differentiate all of the above equations with respect to a typical parameter of interest. In keeping with the remarks at the close of the previous section, we emphasize that differentiation is with respect to $\underline{\epsilon}$ with α and β held fixed.

The mechanics of the differentiation are straightforward but tedious. We represent by capitalized variables the differentiated variables;

$$\Theta = \frac{\partial \theta}{\partial \epsilon} \, , \; S = \frac{\partial s}{\partial \epsilon} \, , \; X = \frac{\partial x}{\partial \epsilon} \, , \; Y = \frac{\partial y}{\partial \epsilon} \, , \; \Psi = \frac{\partial \mu}{\partial \epsilon} \tag{1.13}$$

when (1.4), (1.5), (1.6), and (1.8) are parametrically differentiated we obtain,

$$S_\beta = 0 \tag{1.14}$$

$$\Theta_\alpha + \left[P_{\mu\mu}(\mu)\,\mu_\alpha - \frac{s_\alpha \cos 2\mu}{\gamma}\right]\Psi + P_\mu(\mu)\,\Psi_\alpha - \frac{\sin 2\mu}{2}\,S_\alpha = 0 \tag{1.15}$$

$$\Theta_\beta + \left[\frac{x_\beta \theta_\alpha}{x_\alpha}\sec^2\theta \tan\mu\right]\Theta - (1 - \tan\theta\tan\mu)\frac{x_\beta}{x_\alpha}\,\Theta_\alpha =$$

$$P_\mu(\mu)\,\Psi_\beta + \left[P_{\mu\mu}(\mu)\mu_\beta - \frac{x_\beta \theta_\alpha}{x_\alpha}\sec^2\mu\tan\theta\right]\Psi + (1 - \tan\theta\tan\mu)\frac{\theta_\alpha}{x_\alpha}\left(X_\beta - \frac{x_\beta}{x_\alpha}X_\alpha\right) \tag{1.16}$$

$$Y_\alpha = X_\alpha \tan(\theta + \mu) + X_\alpha \sec^2(\theta + \mu)(\Theta + \Psi) \tag{1.17}$$

$$Y_\beta = X_\beta \tan\theta + X_\beta \sec^2\theta \tag{1.18}$$

It should be noted that we have dropped the specification that ϵ be a vector. This has been done for ease of exposition. This can be done without loss of generality. Variation with respect to each parameter can be treated separately, since only first order variations are being considered.

At the shock the parametrically differentiated equations are

$$\frac{d\eta}{d\epsilon} = \frac{\cos^2\eta}{(x_\alpha + x_\beta)^2}\left[Y_\alpha(x_\alpha + x_\beta) + Y_\beta(x_\alpha + x_\beta) - X_\alpha(y_\alpha + y_\beta) - X_\beta(y_\alpha + y_\beta)\right] \tag{1.19}$$

$$S = \left[\frac{17.5}{6+7w} + \frac{3.5}{6+w} - \frac{3.5}{1+w}\right]\frac{dw}{d\epsilon} \tag{1.20}$$

$$\Psi = \frac{0.2A\left[\frac{4}{3} + \frac{7}{18}w\right] - 0.2\left[1+\frac{7}{6}w\right]\left[1+\frac{1}{6}w\right]\left[0.2M^2 - \frac{1}{3} - \frac{7}{18}w\right]}{A^2 \sin 2\mu}\frac{dw}{d\epsilon} \tag{1.21}$$

where $\frac{dw}{d\epsilon} = M^2 \sin 2\eta \frac{d\eta}{d\epsilon}$, $A = 1+0.2M^2(1+w) - (1+\frac{7}{6}w)(1+\frac{1}{6}w)$

$$\frac{d\theta}{d\epsilon} = \frac{d\eta}{d\epsilon}\cos^2\theta\left\{-\frac{1}{\sin^2\eta}\frac{(M^2-1)\tan^2\eta - 1}{(1+\frac{\gamma+1}{2}M^2) + (1+\frac{\gamma-1}{2}M^2)\tan^2\eta}\right.$$

$$+ \frac{2}{\left[(1+\frac{\gamma+1}{2}M^2) + (1+\frac{\gamma-1}{2}M^2)\tan^2\eta\right]^2}\left[(M^2-1)\sec\eta(1+\frac{\gamma+1}{2}M^2)\right. \tag{1.22}$$

$$\left.\left. + (1+\frac{\gamma-1}{2}M^2)\tan^2\eta\right] - \left[(M^2-1)\tan^2\eta - 1\right](1+\frac{\gamma-1}{2}M^2)\sec^2\eta\right]\right\}$$

In the actual integration (1.21-1.25) are applied at the shock

$$\alpha = \beta \tag{1.23}$$

At the body $\alpha = 0$ the appropriate equations are

$$\underline{X} = 0, \quad \underline{Y} = f\frac{\partial\beta}{\partial\underline{\epsilon}}, \quad \underline{\theta} = \frac{\partial f_\beta(\beta, \epsilon)}{\partial\underline{\epsilon}}\cos^2\theta \tag{1.24}$$

In writing (1.24) we revert to the general case in which many parameters are being considered. At this point we can simultaneously numerically integrate the

non-linear system and the variational equations. The calculation of the base flow is second order accurate [2]. The calculation of the new flow is first order in space, second order in the parameters of interest. The calculation of the two flows is interleaved in that after the flow along β = constant is computed by the base code, the parametric code then calculates the exact derivatives in order to obtain the variational flow.

RESULTS

As we have already mentioned the method applies generally to many independently varying parameters. As a typical use of the variational quantities we use Taylor's theorem to consider the change in pressure,

$$p_{new} \approx p_{base} + \Sigma_i \, (\partial p / \partial \epsilon_{i0})(\epsilon_i - \epsilon_{i0}) \tag{1.25}$$

where ϵ_i represents the various parameters with the differential coefficients calculated holding α and β fixed and the zero subscript denotes a reference or base calculation.

For example, if just thickness is considered and denoted by say ϵ, then at the body

$$p_{new} \approx p_{base} + \left[\frac{\partial p}{\partial \epsilon}\right]_{\alpha=0,\beta} (\epsilon - \epsilon_o) = p_{base} + \left[\left[\frac{\partial p}{\partial \epsilon}\right]_{x,\, y=f} + \left[\frac{\partial p}{\partial y}\right]_{x,\, y=f} \left[\frac{\partial f}{\partial \epsilon}\right]\right](\epsilon - \epsilon_0) \tag{1.26}$$

The second form exhibits the result obtained if variation in the physical plane is considered.

In the numerical calculations that are discussed, we have taken for f a family of shapes given by

$$y = 2\epsilon x(1-x) - x \tan \Delta + 10x\epsilon (x-1)\left(x - \frac{1}{2}\right) c \tag{1.27}$$

Thus, ϵ is the thickness ratio based on chord, Δ the mean chord angle of attack, and c a scaling factor for the camber (shape) function. Figure 3 shows the effect of changing just the thickness (Δ,c = 0). Here we have plotted the pressure distribution

on the upper surface and the airfoil which, for aesthetic reasons, has the lower surface plotted as a reflection of the upper surface. Note that the method gives good agreement with the exact solution even when the new thickness is fifty percent greater than the base thickness.

More generally we consider variations in all three parameters. Thus, the pressure relation at the body is

$$p_{new} \approx p_{base} + \left(\frac{\partial p}{\partial \epsilon}\right)_{\alpha=0,\beta}(\epsilon - \epsilon_o) + \left(\frac{\partial p}{\partial \Delta}\right)_{\alpha=0,\beta}(\Delta - \Delta_o) + \left(\frac{\partial p}{\partial c}\right)_{\alpha=0,\beta}(c - c_0) \qquad (1.28)$$

Figures 4 through 6 show the effect of changing various combinations of thickness, angle of attack, and camber. Here we see that, although the airfoil configurations are markedly different, there is very good agreement between the parametrically generated pressure distribution and the exact pressure distribution for the new airfoil.

INVERSE CASE

The method which has been presented also works as well on the inverse or design problem where the pressure on the body is known, but the shape of the body is to be determined. Using the Bernoulli equation and the perfect gas law one may show [1]

$$\mu = \sin^{-1}\left[\left[\frac{\gamma-1}{2}\,\frac{\exp\left(\frac{\gamma-1}{\gamma}(s + \ln\gamma p)\right)}{1 + \frac{\gamma-1}{2}M^2 - \exp\left(\frac{\gamma-1}{\gamma}(s + \ln\gamma p)\right)}\right]^{1/2}\right] \qquad (1.29)$$

This when differentiated, yields

$$\Psi - \frac{(\gamma-1)^2}{2\gamma}\,\frac{\left(1 + \frac{\gamma-1}{2}M^2\right)\exp(w)}{\left[1+\frac{\gamma-1}{2}M^2 - \exp(w)\right]^2 \sin^2\mu}\,S = \frac{(\gamma-1)^2}{2\gamma}\,\frac{\left(1+\frac{\gamma-1}{2}M^2\right)\exp(w)}{\left[1+\frac{\gamma-1}{2}M^2 - \exp(w)\right]^2 \sin^2\mu}\,\frac{d(\ln p)}{d\epsilon} \qquad (1.30)$$

where

$$w = \frac{\gamma-1}{\gamma}(s + \ln p)$$

Obviously at the airfoil we can no longer use (1.6) since we are hoping to determine the shape of the airfoil. Instead we must use (1.5) and (1.29). Therefore, the parametrically differentiated equations (1.24) must be replaced by (1.17), (1.18) and (1.30). The integration may now proceed as in the direct case [2]. The results of the variational calculations are presented in Figures 7 through 9. Notice that even for a 20% change in the logarithm of the pressure (corresponding to a 50% increase in thickness), the difference between the exact airfoil shape and the computed shape is less than 4%.

FIGURE CAPTIONS

Fig. 1. Body, C+ characteristics, streamlines and C⁻ characteristics (dashed) in physical (x,y) plane, from [1].

Fig. 2. Body, C+ characteristics and streamlines in (α,β) plane.

Fig. 3. Pressure distribution on 10% and 15% thick airfoils at M = 2 and 10% and 15% airfoils.

Fig. 4. Pressure distribution on 10% thick airfoil, uncambered at 0 degree angle of attack and cambered (c=0.1) at 5 degrees angle of attack at M = 2 along with respective bodies.

Fig. 5. Pressure distribution on 10% thick airfoil, uncambered at 0 degree angle of attack and canbered (c=0.2) at 5 degrees angle of attack at M = 2 along with respective bodies.

Fig. 6. Pressure distribution on 10% thick airfoil, uncambered at 0 degree angle of attack and cambered (c=0.2) at 10 degrees angle of attack at M = 2 along with respective bodies.

Fig. 7. Inverse case: pressure distribution on 10% and 12% airfoils, M = 2, along with generated bodies. Dashed airfoil is computed shape.

Fig. 8. Inverse case: pressure distribution on 10% and 15% airfoils, M = 2, along with generated bodies. Dashed airfoil is computed shape.

Fig. 9. Inverse case: pressure distribution on 10% and 12% airfoils, M = 4, along with generated bodies. Dashed airfoil is computed shape.

PHYSICAL PLANE

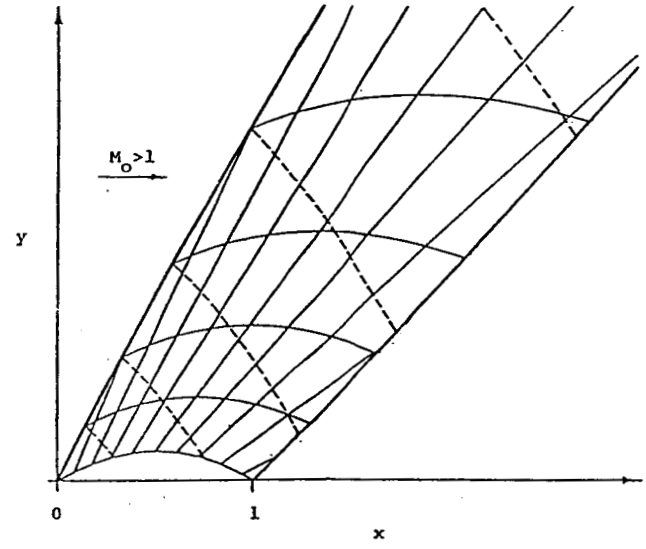

Figure 1

COMPUTATIONAL PLANE

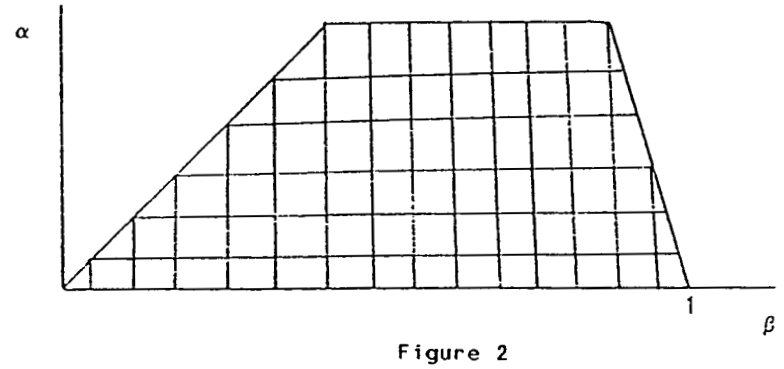

Figure 2

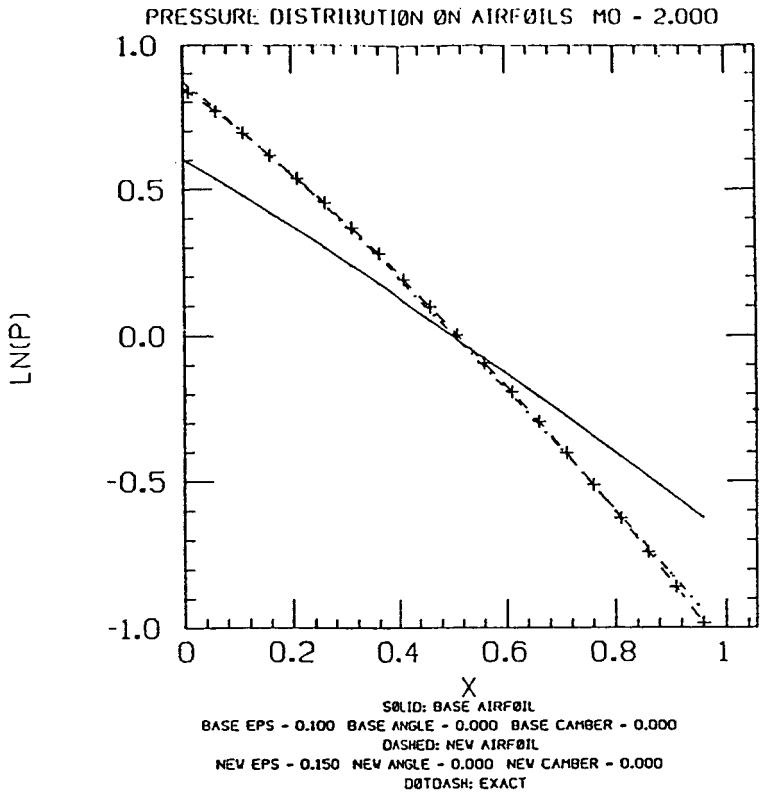
PRESSURE DISTRIBUTION ON AIRFOILS MO - 2.000
1.0
0.5
0.0
-0.5
-1.0
LN(P)
0
0.2
0.4
0.6
0.8
1
X
SOLID: BASE AIRFOIL
BASE EPS - 0.100 BASE ANGLE - 0.000 BASE CAMBER - 0.000
DASHED: NEW AIRFOIL
NEW EPS - 0.150 NEW ANGLE - 0.000 NEW CAMBER - 0.000
DOTDASH: EXACT

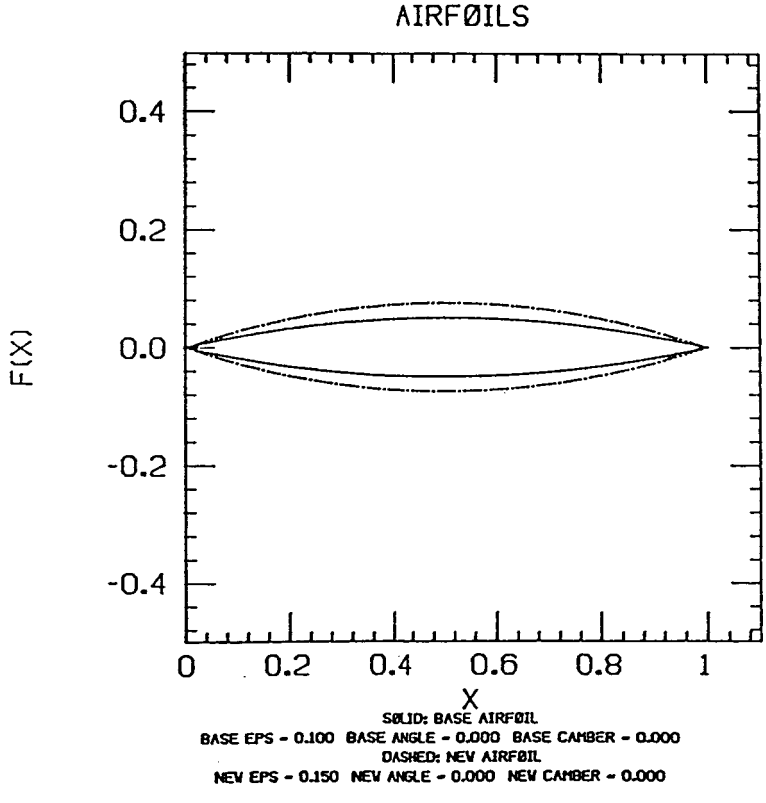
AIRFOILS
0.4
0.2
0.0
-0.2
-0.4
F(X)
0
0.2
0.4
0.6
0.8
1
X
SOLID: BASE AIRFOIL
BASE EPS - 0.100 BASE ANGLE - 0.000 BASE CAMBER - 0.000
DASHED: NEW AIRFOIL
NEW EPS - 0.150 NEW ANGLE - 0.000 NEW CAMBER - 0.000

Figure 3

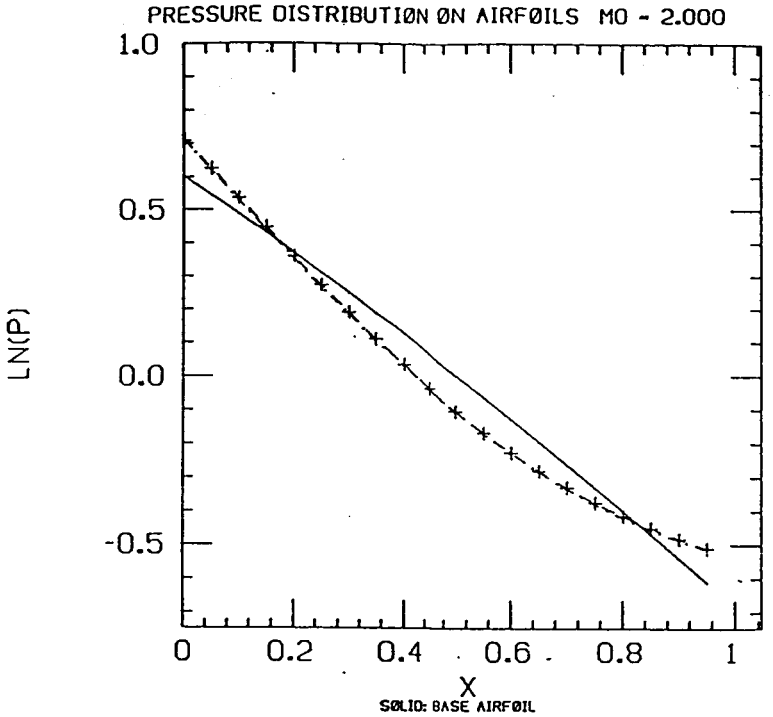
PRESSURE DISTRIBUTIØN ØN AIRFØILS MO - 2.000
LN(P)
1.0
0.5
0.0
-0.5
0
0.2
0.4
0.6
0.8
1
X
SØLID: BASE AIRFØIL
BASE EPS - 0.100 BASE ANGLE - 0.000 BASE CAMBER - 0.000
DASHED: NEW AIRFØIL
NEW EPS - 0.100 NEW ANGLE - 0.087 NEW CAMBER - 0.100
DØTDASH: EXACT SØLN

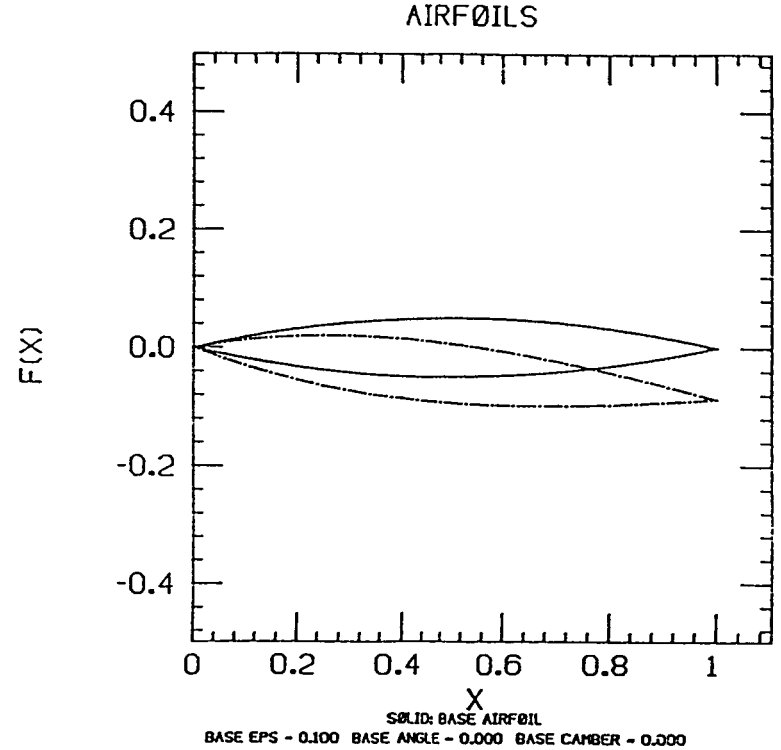
AIRFØILS
F(X)
0.4
0.2
0.0
-0.2
-0.4
0
0.2
0.4
0.6
0.8
1
X
SØLID: BASE AIRFØIL
BASE EPS - 0.100 BASE ANGLE - 0.000 BASE CAMBER - 0.000
DASHED: NEW AIRFØIL
NEW EPS - 0.100 NEW ANGLE - 0.087 NEW CAMBER - 0.100

Figure 4

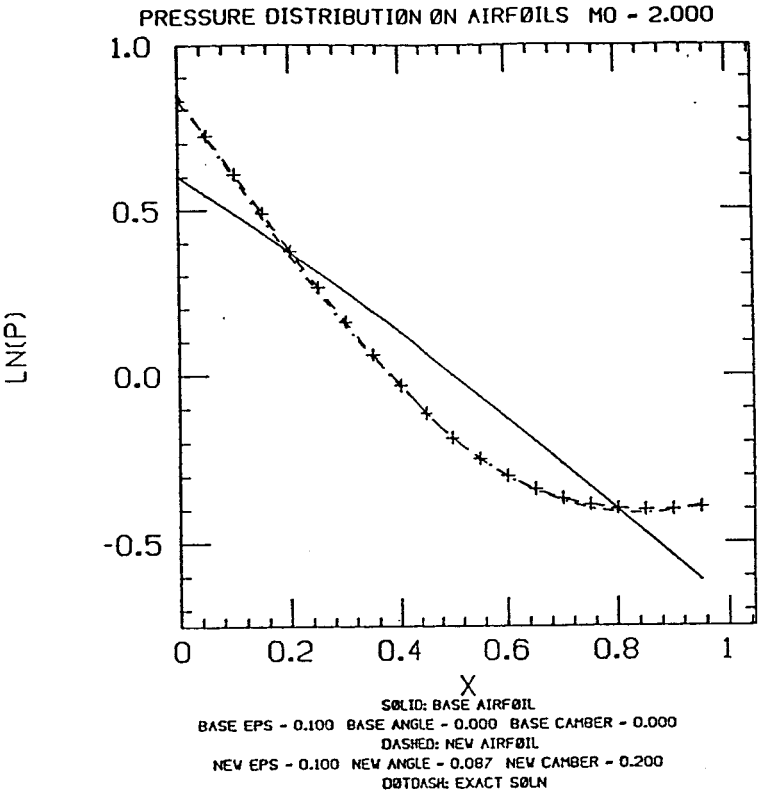
PRESSURE DISTRIBUTIØN ØN AIRFØILS MO - 2.000
LN(P)
1.0
0.5
0.0
-0.5
0
0.2
0.4
0.6
0.8
1
X
SØLID: BASE AIRFØIL
BASE EPS - 0.100 BASE ANGLE - 0.000 BASE CAMBER - 0.000
DASHED: NEW AIRFØIL
NEW EPS - 0.100 NEW ANGLE - 0.087 NEW CAMBER - 0.200
DØTDASH: EXACT SØLN

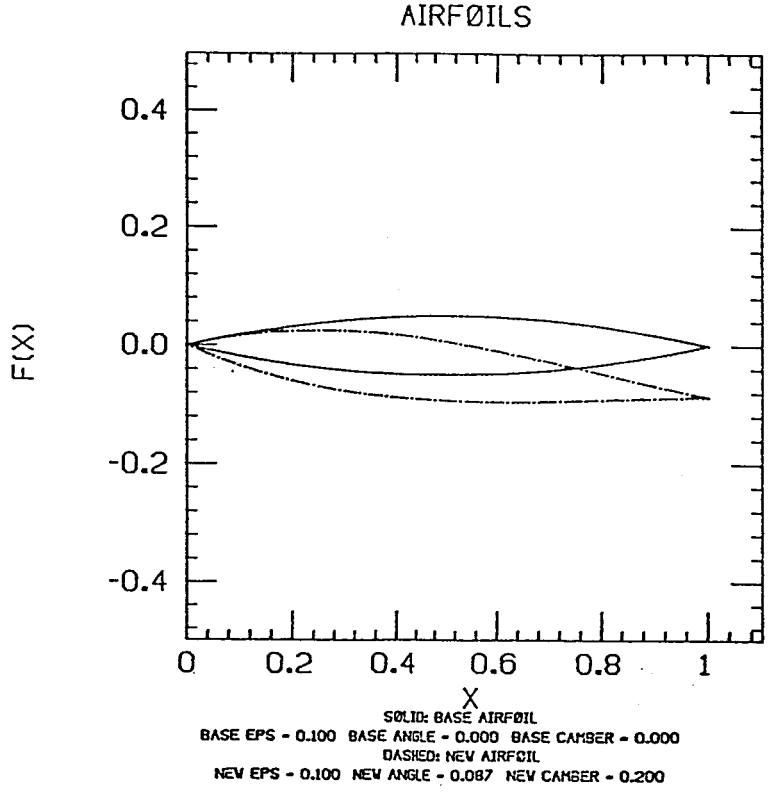
AIRFØILS
F(X)
0.4
0.2
0.0
-0.2
-0.4
0
0.2
0.4
0.6
0.8
1
X
SØLID: BASE AIRFØIL
BASE EPS - 0.100 BASE ANGLE - 0.000 BASE CAMBER - 0.000
DASHED: NEW AIRFØIL
NEW EPS - 0.100 NEW ANGLE - 0.087 NEW CAMBER - 0.200

Figure 5

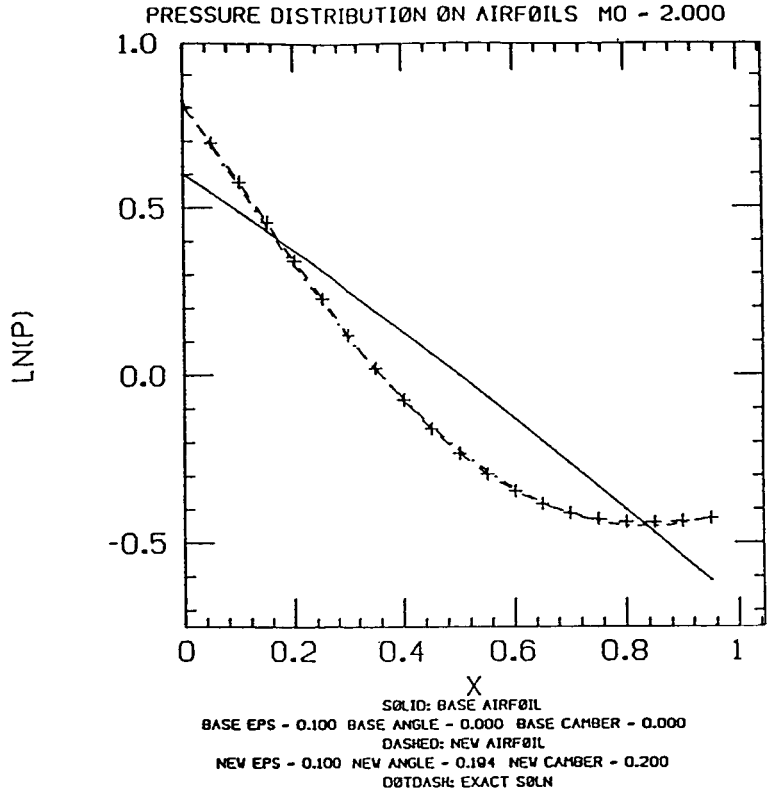
PRESSURE DISTRIBUTIØN ØN AIRFØILS MO - 2.000
1.0
0.5
0.0
-0.5
LN(P)
0
0.2
0.4
0.6
0.8
1
X
SØLID: BASE AIRFØIL
BASE EPS - 0.100 BASE ANGLE - 0.000 BASE CAMBER - 0.000
DASHED: NEW AIRFØIL
NEW EPS - 0.100 NEW ANGLE - 0.194 NEW CAMBER - 0.200
DØTDASH: EXACT SØLN

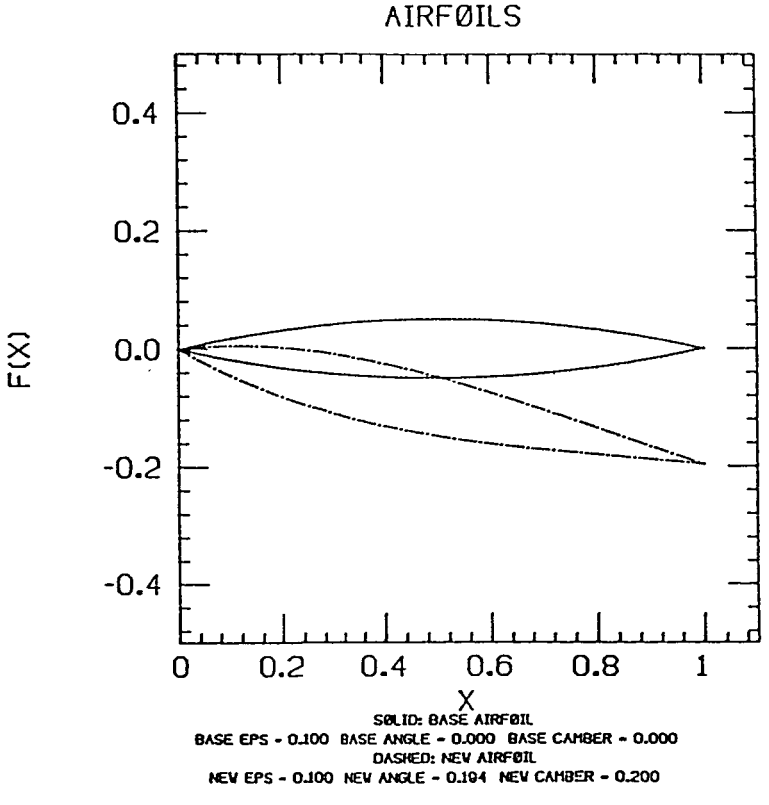
AIRFØILS
0.4
0.2
0.0
-0.2
-0.4
F(X)
0
0.2
0.4
0.6
0.8
1
X
SØLID: BASE AIRFØIL
BASE EPS - 0.100 BASE ANGLE - 0.000 BASE CAMBER - 0.000
DASHED: NEW AIRFØIL
NEW EPS - 0.100 NEW ANGLE - 0.194 NEW CAMBER - 0.200

Figure 6

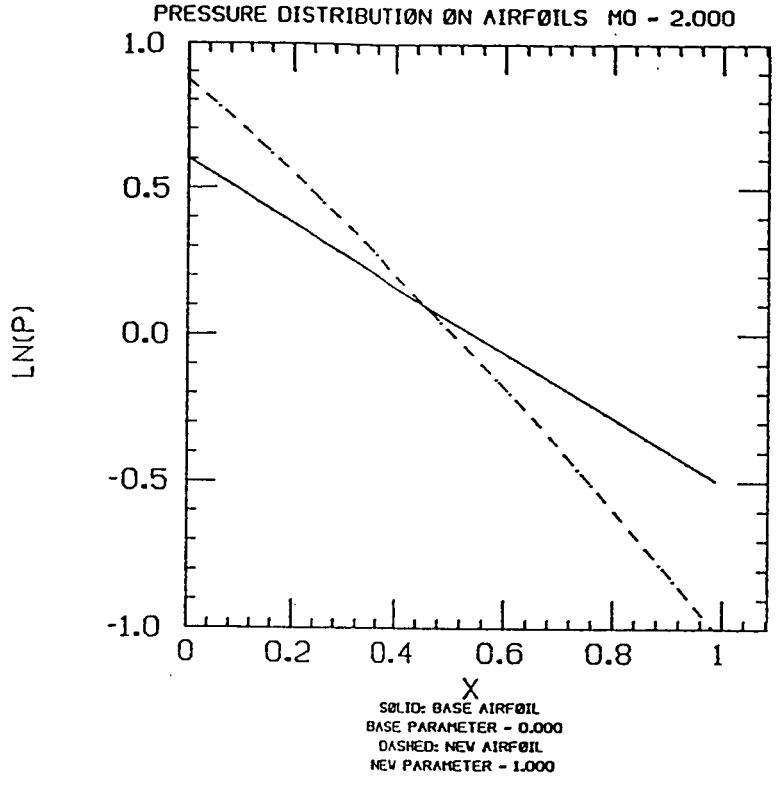
PRESSURE DISTRIBUTIØN ØN AIRFØILS MO - 2.000
1.0
0.5
0.0
-0.5
-1.0
LN(P)
0
0.2
0.4
0.6
0.8
1
X
SØLID: BASE AIRFØIL
BASE PARAMETER - 0.000
DASHED: NEW AIRFØIL
NEW PARAMETER - 1.000

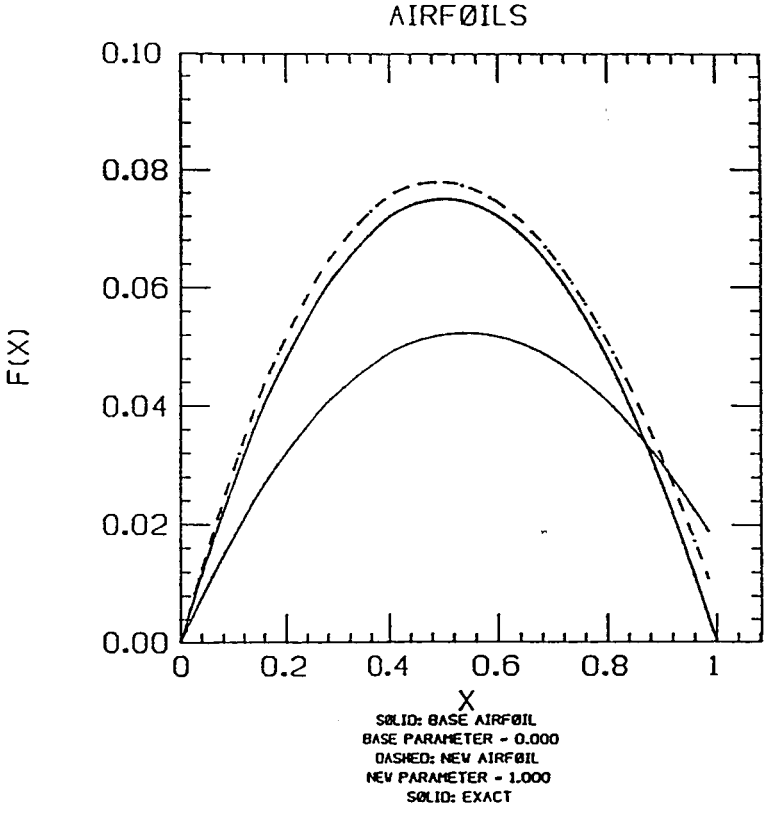
AIRFØILS
0.10
0.08
0.06
0.04
0.02
0.00
F(X)
0
0.2
0.4
0.6
0.8
1
X
SØLID: BASE AIRFØIL
BASE PARAMETER - 0.000
DASHED: NEW AIRFØIL
NEW PARAMETER - 1.000
SØLID: EXACT

Figure 7

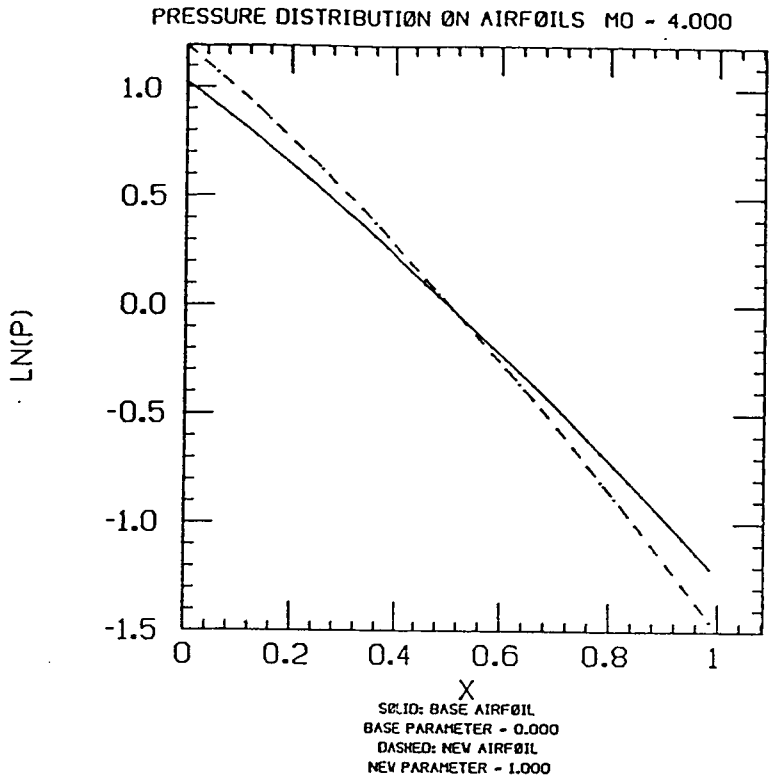
PRESSURE DISTRIBUTIØN ØN AIRFØILS MO - 4.000
LN(P)
1.0
0.5
0.0
-0.5
-1.0
-1.5
0
0.2
0.4
0.6
0.8
1
X
SØLID: BASE AIRFØIL
BASE PARAMETER - 0.000
DASHED: NEW AIRFØIL
NEW PARAMETER - 1.000

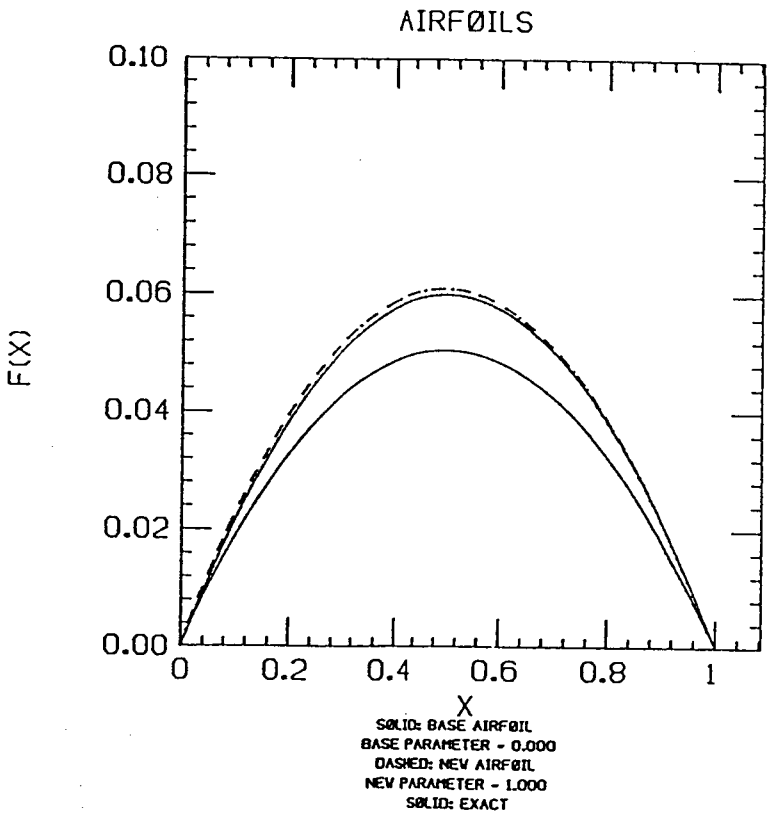
AIRFØILS
F(X)
0.10
0.08
0.06
0.04
0.02
0.00
0
0.2
0.4
0.6
0.8
1
X
SØLID: BASE AIRFØIL
BASE PARAMETER - 0.000
DASHED: NEW AIRFØIL
NEW PARAMETER - 1.000
SØLID: EXACT

Figure 8

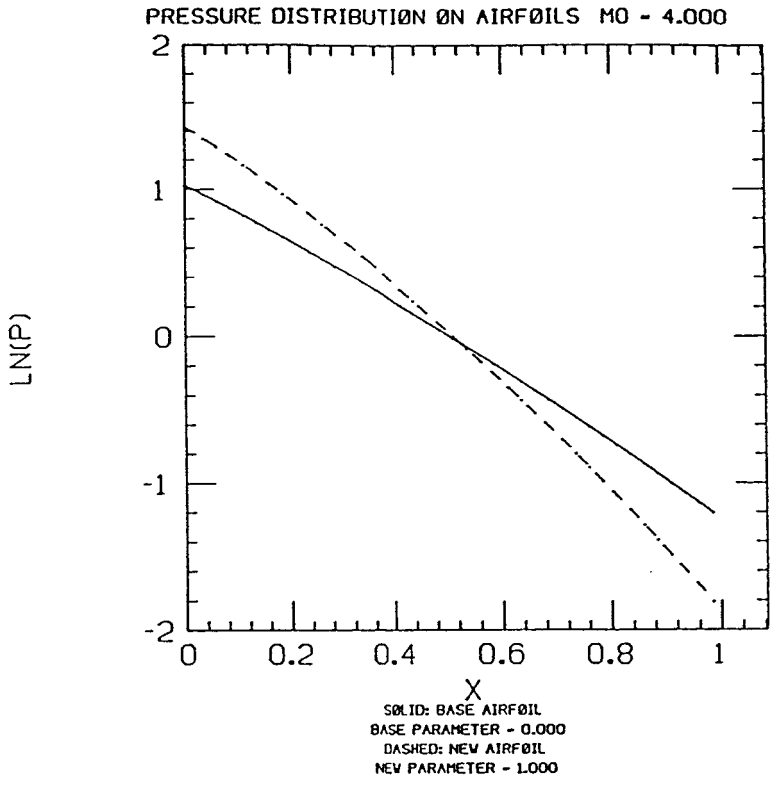
PRESSURE DISTRIBUTIØN ØN AIRFØILS MO - 4.000
LN(P)
2
1
0
-1
-2
0
0.2
0.4
0.6
0.8
1
X
SØLID: BASE AIRFØIL
BASE PARAMETER - 0.000
DASHED: NEW AIRFØIL
NEW PARAMETER - 1.000

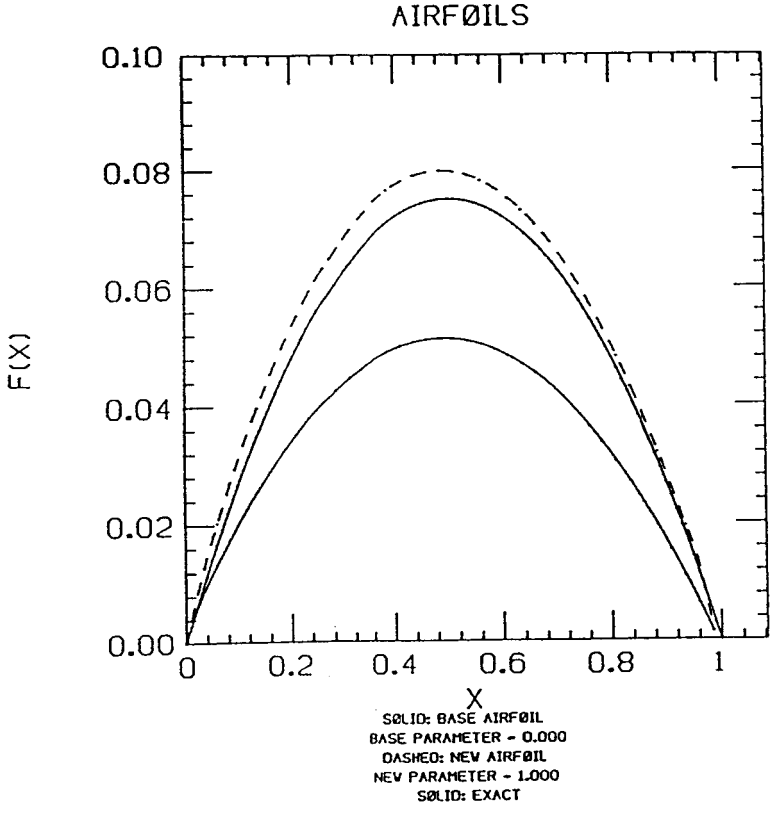
AIRFØILS
F(X)
0.10
0.08
0.06
0.04
0.02
0.00
0
0.2
0.4
0.6
0.8
1
X
SØLID: BASE AIRFØIL
BASE PARAMETER - 0.000
DASHED: NEW AIRFØIL
NEW PARAMETER - 1.000
SØLID: EXACT

Figure 9

REFERENCES

[1] Lewis, T.S. and Sirovich, L., **"Approximate and Exact Numerical Computation of Supersonic Flow Over an Airfoil"**, J. Fluid Mechanics Vol 112, 1981, pp. 265-282.

[2] Fong, J. and Sirovich, L. **"Direct and Invese Problem in Supersonic Axisymmetric Flow"**, AIAA Journal, 24, 5 May 1986.

Chapter II

The Application of the Jacobi Matrix Technique to Axisymmetric Supersonic Flow

"Curiouser and curiouser!" cried Alice (she was so much surprised, that for the moment she quite forgot how to speak good English).

- **Alice's Adventures in Wonderland**
Lewis Carroll

APPLICATION TO AXISYMMETRIC SUPERSONIC FLOW

As another illustration of this method, we consider steady, inviscid, supersonic flows past axisymmetric bodies. For this purpose consider a family of profiles depending on two parameters, thickness and taper. As in Chapter 1, we shall summarize the methods used in solving such flows [1], [2]. The equations are written in characteristic form as follows:

$$s_\beta = 0 \tag{2.1}$$

$$(\theta + P(\mu))_\alpha = \frac{\sin 2\mu}{2\gamma} s'(\alpha) - \frac{\tan\theta \tan\mu}{\tan\theta + \tan\mu} \frac{r_\alpha}{r} \tag{2.2}$$

$$(\theta - P(\mu))_\beta = (1 - \tan\theta \tan\mu) \frac{x_\beta}{x_\alpha} \theta_\alpha + \tan\mu \frac{r_\beta}{r} \tag{2.3}$$

Here the coordinates (α,β) correspond to the streamlines, α = constant, and the C^+ characteristics, β = constant (Figure 1). θ is the flow deflection angle, μ is the Mach angle and s is the entropy. $P(\mu)$ is the Prandtl function given by

$$P(\mu) = \lambda^{1/2} \tan^{-1}(\lambda^{1/2} \tan\mu) - \mu \ , \ \lambda = (\gamma+1)/(\gamma-1) \ . \tag{2.4}$$

As in the two-dimensional case, these equations are exact and are valid in the hypersonic flow regime so long as such real gas effects as disassociation and ionization can be ignored. The physical coordinates x,r satisfy the relations [1], [2]

$$r_\alpha = x_\alpha \tan(\theta+\mu), \qquad r_\beta = x_\beta \tan\theta \tag{2.5}$$

As with Chapter 1, the transformation to (α,β) coordinates leaves open two arbitrary functions; these are fixed so that the shock is along $\alpha = \beta$ and the body is positioned along the line $\alpha = 0$ (Figure 2). Hence, we have a body fit, shock fit coordinate system. The boundary conditions at the body are

$$x(0,\beta) = \beta, \quad r(0,\beta) = f(\beta,\underline{\epsilon}) \ , \quad \theta(0,\beta) = \tan^{-1}(f_\beta(\beta), \underline{\epsilon}) \ . \tag{2.6}$$

The Rankine-Hugoniot conditions govern the jumps in θ, μ and s at the shock. Written in terms of the shock angle η, they are given by

$$\tan\theta = \frac{1}{\tan\eta} \frac{(M^2 - 1)\tan^2\eta - 1}{(1+\frac{\gamma+1}{2}M^2) + (1+\frac{\gamma-1}{2}M^2)\tan^2\eta} \tag{2.7}$$

$$\sin^2\mu = \frac{0.2(1+\frac{7}{6}w)(1+\frac{1}{6}w)}{(1+w)(1+0.2M^2) - (1+\frac{7}{6}w)(1+\frac{1}{6}w)} \tag{2.8}$$

$$s = 2.5 \ln(1+\frac{7}{6}w) + 3.5 \ln(1+\frac{1}{6}w) - 3.5 \ln(1+w) \tag{2.9}$$

where

$$w = M^2\sin^2\eta - 1 \tag{2.10}$$

The shock angle η is related to the coordinates as follows

$$\tan\eta = dr/dx \Big|_{shock} = \frac{r_\alpha + r_\beta}{x_\alpha + x_\beta}\Big|_{shock} \tag{2.11}$$

We have assumed a perfect gas with constant specific heats and hence that

$$p = \rho^\gamma \exp[(\gamma - 1)s] \tag{2.12}$$

It should be noted that this formulation eliminates the difficulty mentioned in the Introduction. For by using the (α,β) - coordinate system, a quantity such as

$$\frac{\partial p}{\partial \underline{\epsilon}}(\alpha, \beta; \underline{\epsilon})$$

signifies the variation with $\underline{\epsilon}$ at fixed α and β. In particular it gives the variation of pressure say fixed at the body or at the shock. This makes the integration of the differential equations significantly simpler.

VARIATIONAL EQUATIONS

As in Chapter 1, we differentiate the governing equations with respect to the parameter of interest, keeping the coordinates α and β held fixed. The differentiation although straightforward is tedious. If we write

$$\Theta = \frac{\partial\theta}{\partial\epsilon}\,,\quad S = \frac{\partial s}{\partial\epsilon}\,,\quad X = \frac{\partial x}{\partial\epsilon}\,,\quad R = \frac{\partial r}{\partial\epsilon}\,,\quad \Psi = \frac{\partial\mu}{\partial\epsilon} \tag{2.13}$$

and parametrically differentiate (2.1), (2.2), (2.3) and (2.5) we then obtain,

$$S_\beta = 0 \tag{2.14}$$

$$\Theta_\alpha + \left[P_{\mu\mu}(\mu)\,\mu_\alpha - \frac{s_\alpha \cos 2\mu}{\gamma} + \frac{r_\alpha \tan^2\theta \sec^2\mu}{r(\tan\theta + \tan\mu)^2}\right]\Psi + P_\mu(\mu)\,\Psi_\alpha - \frac{\sin 2\mu}{2}\,S_\alpha$$

$$+ \frac{r_\alpha \sec^2\theta \tan^2\mu}{r(\tan\theta + \tan\mu)^2}\,\Theta - \frac{r_\alpha \tan\theta \tan\mu}{r^2(\tan\theta + \tan\mu)}\,R = 0 \tag{2.15}$$

$$\Theta_\beta + \left[\frac{x_\beta}{x_\alpha}\theta_\alpha \sec^2\theta \tan\mu\right]\Theta - (1 - \tan\theta\tan\mu)\frac{x_\beta}{x_\alpha}\,\Theta_\alpha =$$

$$P_\mu(\mu)\,\Psi_\beta + \left[P_{\mu\mu}(\mu)\mu_\beta - \frac{x_\beta\theta_\alpha}{x_\alpha}\sec^2\mu\tan\theta + \frac{r_\beta}{r}\sec^2\mu\right]\Psi$$

$$+ (1 - \tan\theta\tan\mu)\frac{\theta_\alpha}{x_\alpha}\left(X_\beta - \frac{x_\beta}{x_\alpha}X_\alpha\right) + \frac{\tan\mu}{r}\,R_\beta - \frac{r_\beta\tan\mu}{r^2}\,R \tag{2.16}$$

$$R_\alpha = X_\alpha \tan(\theta + \mu) + X_\alpha \sec^2(\theta + \mu)(\Theta + \Psi) \tag{2.17}$$

$$R_\beta = X_\beta \tan\theta + X_\beta \sec^2\theta \tag{2.18}$$

At the shock the parametrically differentiated equations are

$$\frac{d\eta}{d\epsilon} = \frac{\cos^2\eta}{(x_\alpha + x_\beta)^2}\left[R_\alpha(x_\alpha + x_\beta) + R_\beta(x_\alpha + x_\beta) - X_\alpha(r_\alpha + r_\beta)\right.$$

$$\left. - X_\beta(r_\alpha + r_\beta)\right] \tag{2.19}$$

$$S = \left[\frac{17.5}{6+7w} + \frac{3.5}{6+w} - \frac{3.5}{1+w}\right] \frac{dw}{d\epsilon} \tag{2.20}$$

$$\Psi = \frac{0.2A\left[\frac{4}{3} + \frac{7}{18}w\right] - 0.2\left[1+\frac{7}{6}w\right]\left[1+\frac{1}{6}w\right]\left[0.2M^2 - \frac{1}{3} - \frac{7}{18}w\right]}{A^2 \sin 2\mu} \frac{dw}{d\epsilon} \tag{2.21}$$

where $\frac{dw}{d\epsilon} = M^2 \sin 2\eta \frac{d\eta}{d\epsilon}$, $A = 1+0.2M^2(1+w) - (1+\frac{7}{6}w)(1+\frac{1}{6}w)$

$$\frac{d\theta}{d\epsilon} = \frac{d\eta}{d\epsilon} \cos^2\theta \left\{ - \frac{1}{\sin^2\eta} \frac{(M^2-1)\tan^2\eta - 1}{(1+\frac{\gamma+1}{2}M^2) + (1+\frac{\gamma-1}{2}M^2)\tan^2\eta} \right. \tag{2.22}$$

$$+ \frac{2}{[(1+\frac{\gamma+1}{2}M^2) + (1+\frac{\gamma-1}{2}M^2)\tan^2\eta]^2} \left[(M^2-1)\sec\eta(1+\frac{\gamma+1}{2}M^2)\right.$$

$$\left.\left. +(1+\frac{\gamma-1}{2}M^2)\tan^2\eta\right] - \left[(M^2-1)\tan^2\eta - 1\right](1+\frac{\gamma-1}{2}M^2)\sec^2\eta\right] \Big\}$$

In the actual integration (2.18-2.22) are applied at the shock

$$\alpha = \beta \tag{2.23}$$

At the body $\alpha = 0$ the appropriate equations are

$$\underline{X} = 0, \quad \underline{R} = f \frac{\partial\beta}{\partial\underline{\epsilon}}, \quad \underline{\theta} = \frac{\partial f_\beta(\beta,\epsilon)}{\partial\underline{\epsilon}} \cos^2\theta \tag{2.24}$$

In writing (2.24) we revert to the general case in which many parameters are being considered. Now we simultaneously numerically integrate the non-linear system and the variational equations. The calculation of the base flow is second order accurate [2]. The calculation of the new flow is first order in space, second order in the parameters of interest. The calculation of the two flows is interleaved in that after the flow along $\beta = 0$ constant is computed by the base code, the parametric code then calculates the exact derivatives in order to obtain the variational flow.

RESULTS

In the numerical calculations discussed, we have taken for f a family of shapes given by

$$r = 2\epsilon x(1-x) + 10x\epsilon (x-1)\ (x - \frac{1}{2})\ c \qquad (2.25)$$

Here we have taken ϵ to be the thickness ratio based on chord, and c as a scaling factor for the taper function.

Figure 3 shows the effect of changing just the thickness (c = 0). Here we have plotted the pressure distribution on the upper surface and the body which, for aesthetics, has the lower surface plotted as a reflection of the upper surface. Note that the method gives good agreement with the exact solution even when the new thickness is 50% more than the base thickness.

Figure 4 shows the effect of changing a combination of thickness, and taper. Here we see that, although the body configurations are markedly different, there is very good agreement between the parametrically generated pressure distribution and the exact pressure distribution for the new body.

INVERSE CASE

The method which has been presented also works quite well in the inverse or design problem where the pressure on the body is known, but the shape of the body shape is to be determined.

Using the Bernoulli equation and the perfect gas law one may show [1]

$$\mu = \sin^{-1}\left[\left[\frac{\gamma-1}{2}\ \frac{\exp\left(\frac{\gamma-1}{\gamma}\ (s + \ln\gamma p)\right)}{1 + \frac{\gamma-1}{2}M^2 - \exp\left(\frac{\gamma-1}{\gamma}\ (s + \ln\gamma p)\right)}\right]^{1/2}\right] \qquad (2.26)$$

This when differentiated, yields

$$\Psi - \frac{(\gamma-1)^2}{2\gamma} \frac{(1+\frac{\gamma-1}{2}M^2)\exp(w)}{\left[1+\frac{\gamma-1}{2}M^2 - \exp(w)\right]^2 \sin^2\mu} S = \frac{(\gamma-1)^2}{2\gamma} \frac{(1+\frac{\gamma-1}{2}M^2)\exp(w)}{\left[1+\frac{\gamma-1}{2}M^2 - \exp(w)\right]^2 \sin^2\mu} \frac{d(\ln p)}{d\epsilon} \quad (2.27)$$

Where

$$w = \frac{\gamma-1}{\gamma}(s+\ln p)$$

At the body, equation (2.6) is no longer valid since we are attempting to determine the shape of the body. Instead we must use (2.5) and (2.26). Therefore, the parametrically differentiated equations (2.24) must be replaced by (2.17), (2.18) and (2.27). The integration may now proceed as in the direct case [2]. The results of the variational calculations are presented in Figures 5 and 6. Notice that even for a 10% change in the logarithm of the pressure (corresponding to a 20% increase in thickness), the difference between the exact body shape and the computed shape is less than 1%.

FIGURE CAPTIONS

Fig. 1 Body, C+ characteristics, streamlines and C⁻ characteristics (dashed) in physical (x,y) plane, from [1].

Fig. 2. Body, C+ characteristics and streamlines in (α,β) plane.

Fig. 3. Pressure distribution on 25% and 30% thick bodies at M = 6 and the respective bodies.

Fig. 4. Pressure distribution on untapered, 25% thick body and 0.10 taper, 30% thick bodies at M = 6 and the respective bodies.

Fig. 5. Inverse case: Pressure distribution on 25% and 30% thick bodies, M = 4 along with generated bodies. Dashed body is computed shape.

Fig. 6. Inverse case: Pressure distribution on 25% and 30% thick bodies, M = 6 along with generated bodies. Dashed body is computed shape.

PHYSICAL PLANE

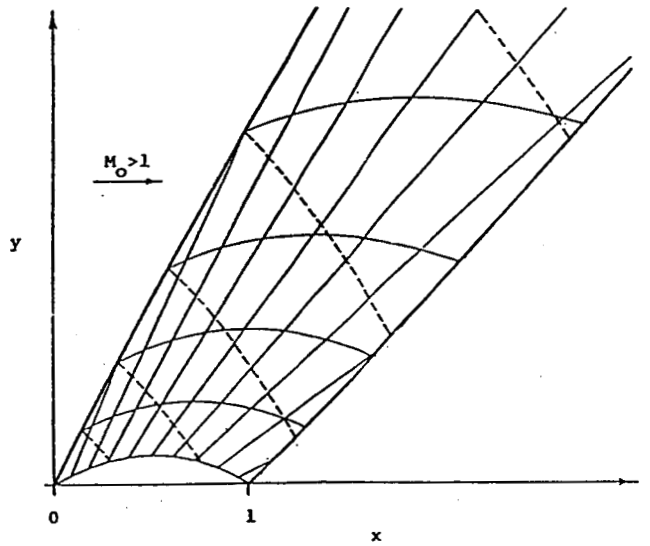

Figure 1

COMPUTATIONAL PLANE

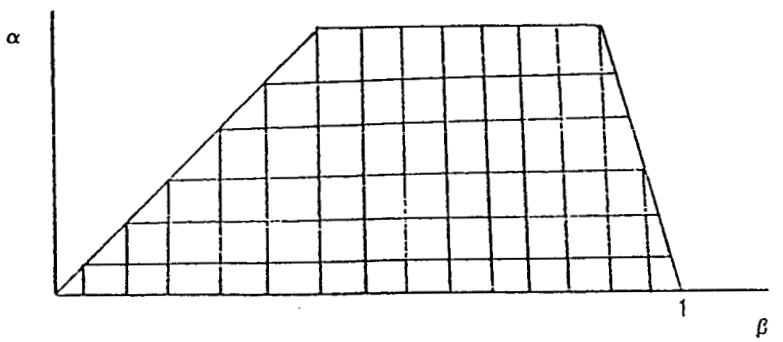

Figure 2

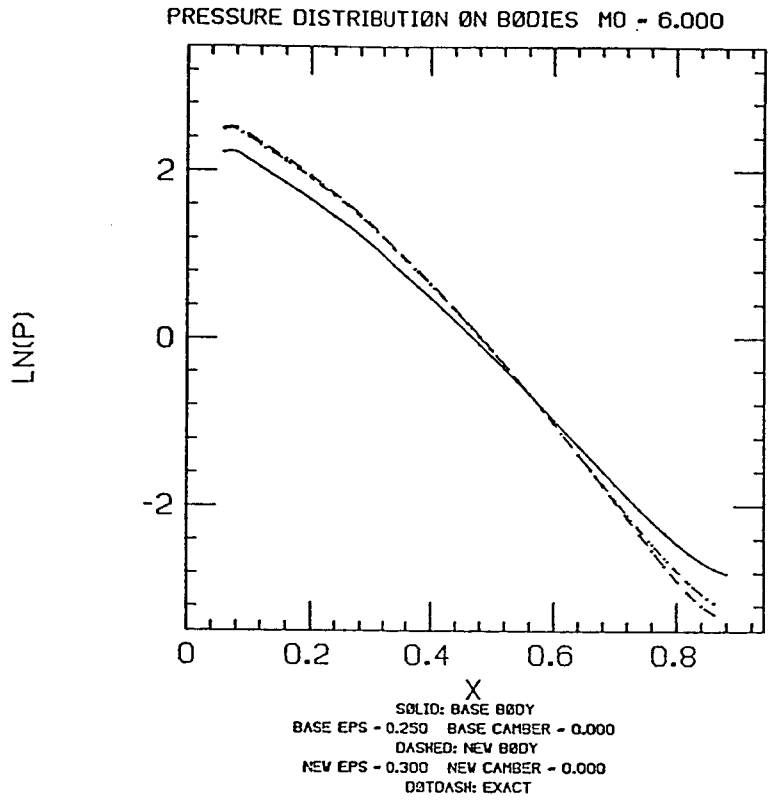
PRESSURE DISTRIBUTIØN ØN BØDIES MO - 6.000
LN(P)
2
0
-2
0
0.2
0.4
0.6
0.8
X
SØLID: BASE BØDY
BASE EPS - 0.250 BASE CAMBER - 0.000
DASHED: NEW BØDY
NEW EPS - 0.300 NEW CAMBER - 0.000
DØTDASH: EXACT

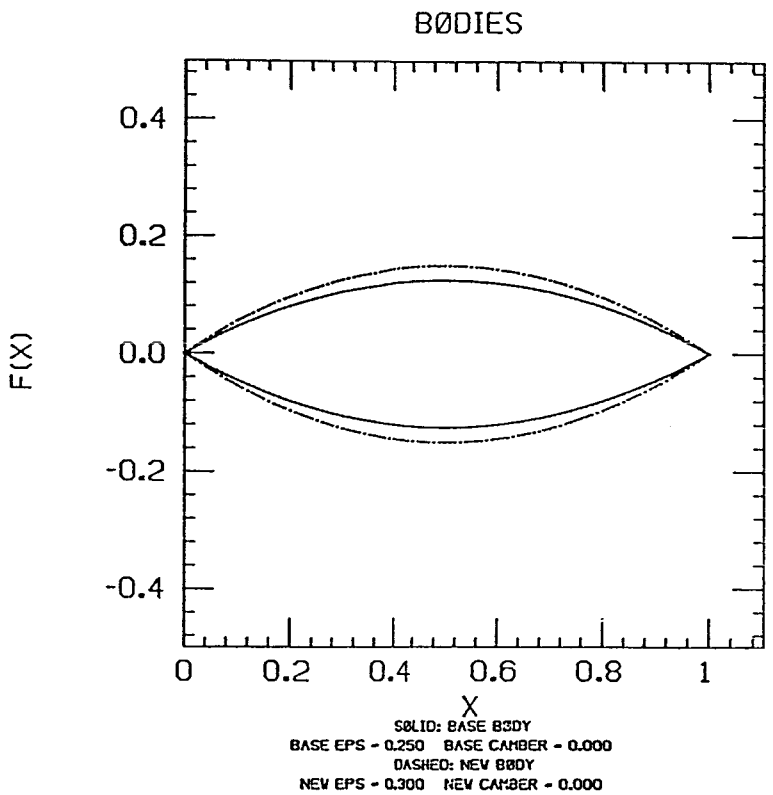
BØDIES
F(X)
0.4
0.2
0.0
-0.2
-0.4
0
0.2
0.4
0.6
0.8
1
X
SØLID: BASE BØDY
BASE EPS - 0.250 BASE CAMBER - 0.000
DASHED: NEW BØDY
NEW EPS - 0.300 NEW CAMBER - 0.000

Figure 3

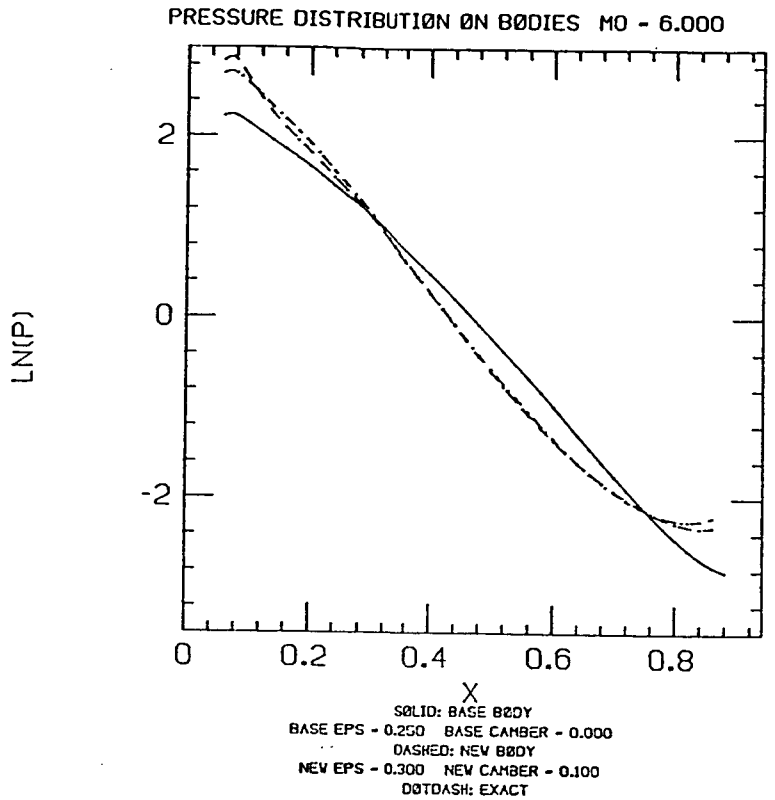
PRESSURE DISTRIBUTIØN ØN BØDIES MO - 6.000
LN(P)
2
0
-2
0
0.2
0.4
0.6
0.8
X
SØLID: BASE BØDY
BASE EPS - 0.250 BASE CAMBER - 0.000
DASHED: NEW BØDY
NEW EPS - 0.300 NEW CAMBER - 0.100
DØTDASH: EXACT

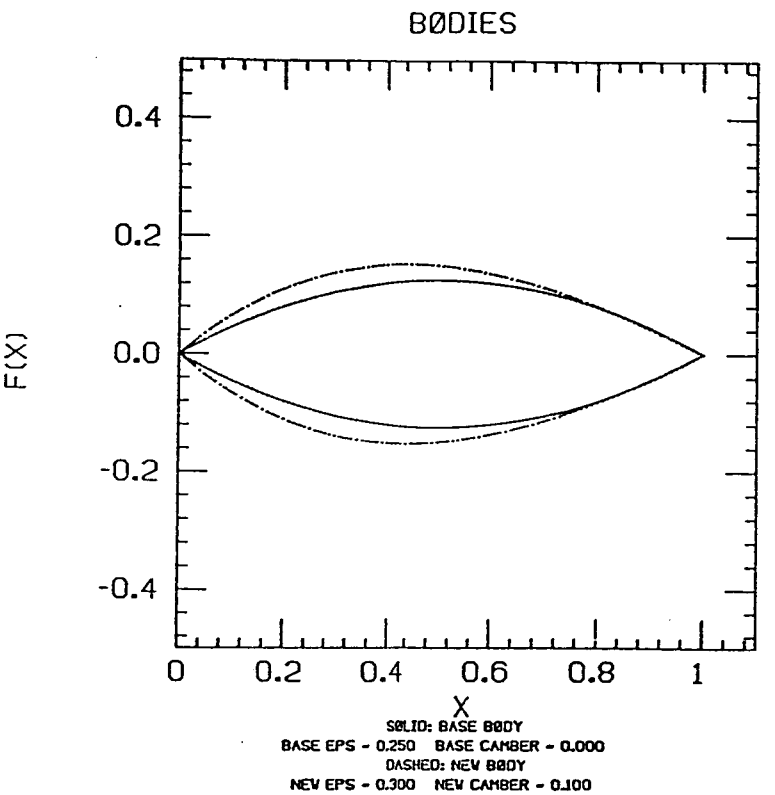
BØDIES
F(X)
0.4
0.2
0.0
-0.2
-0.4
0
0.2
0.4
0.6
0.8
1
X
SØLID: BASE BØDY
BASE EPS - 0.250 BASE CAMBER - 0.000
DASHED: NEW BØDY
NEW EPS - 0.300 NEW CAMBER - 0.100

Figure 4

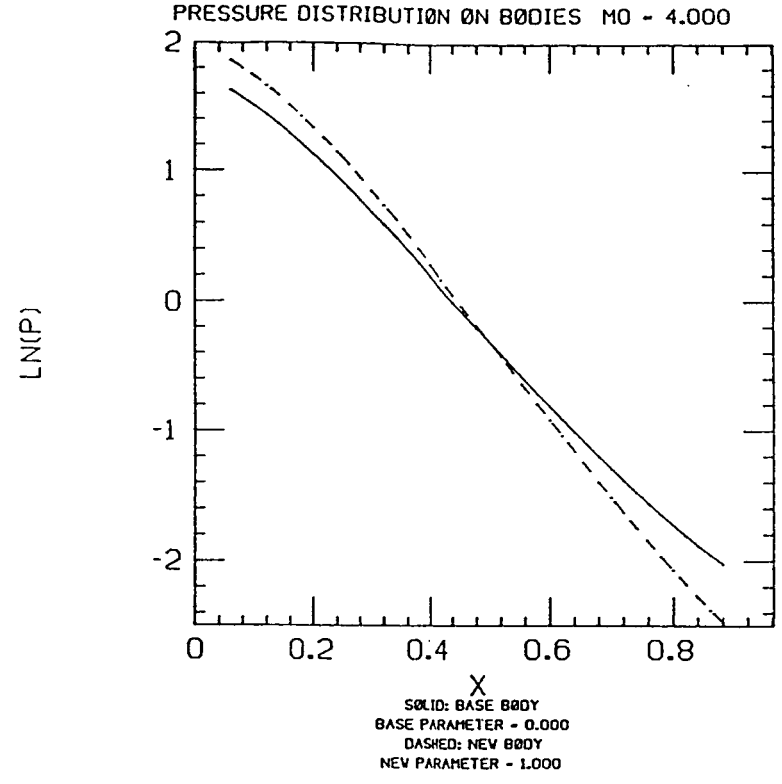
PRESSURE DISTRIBUTIØN ØN BØDIES MO - 4.000
LN(P)
2
1
0
-1
-2
0
0.2
0.4
0.6
0.8
X
SØLID: BASE BØDY
BASE PARAMETER - 0.000
DASHED: NEW BØDY
NEW PARAMETER - 1.000

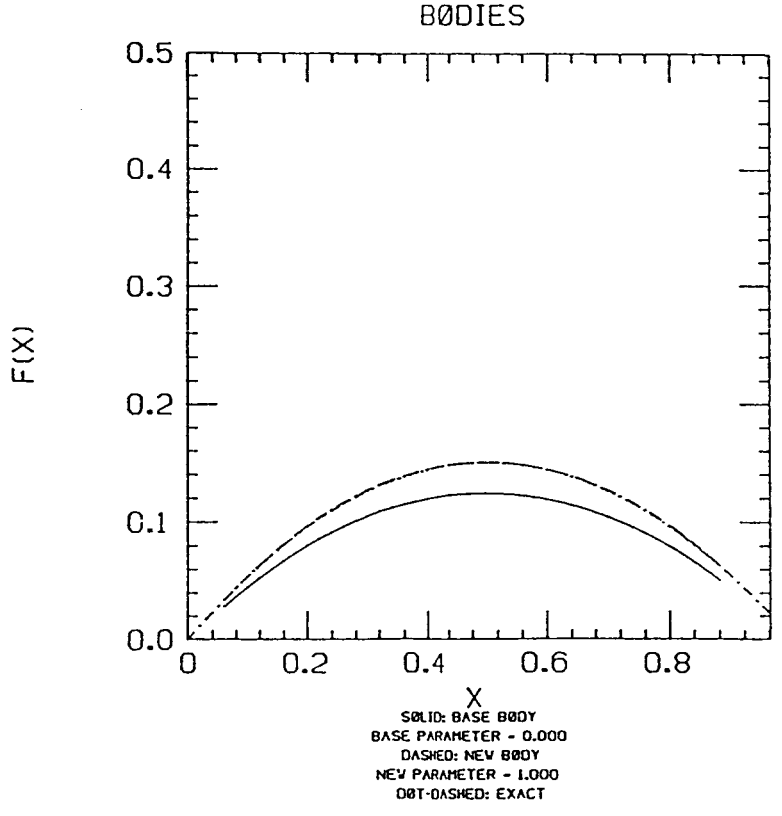
BØDIES
F(X)
0.5
0.4
0.3
0.2
0.1
0.0
0
0.2
0.4
0.6
0.8
X
SØLID: BASE BØDY
BASE PARAMETER - 0.000
DASHED: NEW BØDY
NEW PARAMETER - 1.000
DØT-DASHED: EXACT

Figure 5

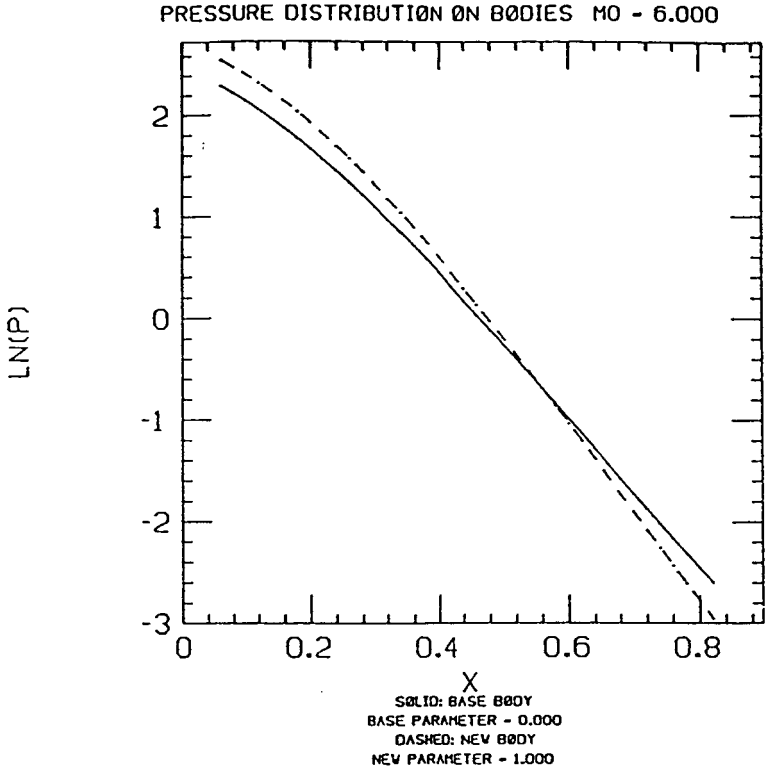
PRESSURE DISTRIBUTIØN ØN BØDIES MO - 6.000
LN(P)
2
1
0
-1
-2
-3
0
0.2
0.4
0.6
0.8
X
SØLID: BASE BØDY
BASE PARAMETER - 0.000
DASHED: NEW BØDY
NEW PARAMETER - 1.000

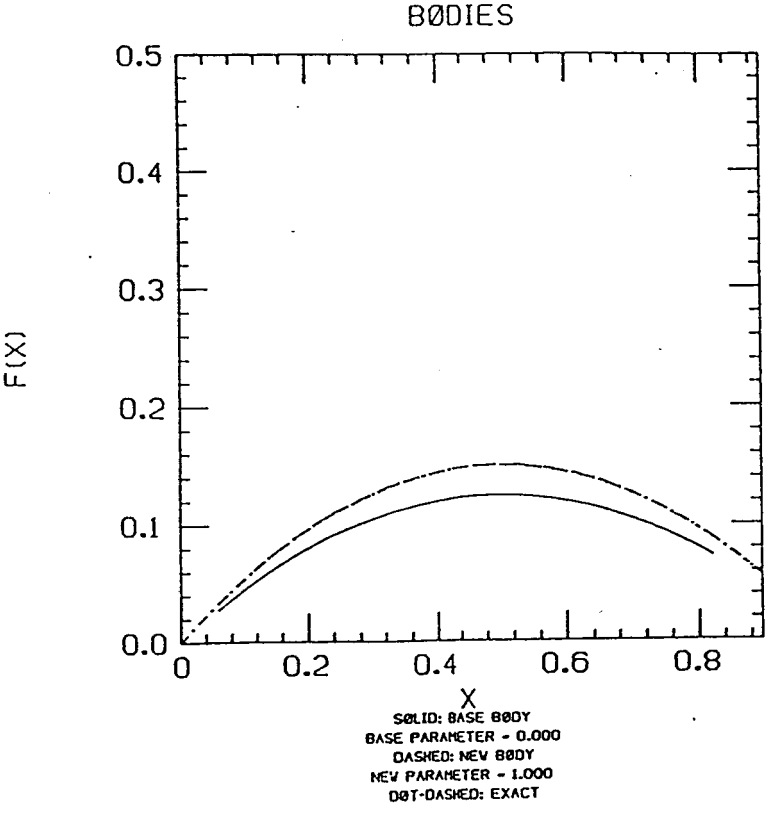
BØDIES
F(X)
0.5
0.4
0.3
0.2
0.1
0.0
0
0.2
0.4
0.6
0.8
X
SØLID: BASE BØDY
BASE PARAMETER - 0.000
DASHED: NEW BØDY
NEW PARAMETER - 1.000
DØT-DASHED: EXACT

Figure 6

REFERENCES

[1] Lewis, T.S. and Sirovich, L., **"Approximate and Exact Numerical Computation of Supersonic Flow Over an Airfoil"**, J. Fluid Mechanics Vol 112, 1981, pp. 265-282.

[2] Fong, J. and Sirovich, L. **"Direct and Inverse Problem in Supersonic Axisymmetric Flow"**, AIAA Journal, 4, 5 May 1986.

Chapter III

The Jacobi Matrix Method for General Flows

Here one of the guinea-pigs cheered, and was immediately suppressed by the officers of the court.

- **Alice's Adventures in Wonderland**
Lewis Carroll

DIRECT DIFFERENCING

The procedure outlined in Chapters 1 and 2 holds in much greater generality than we have considered. The Jacobi matrix technique could also be applied to unsteady flows and to viscous flows in three dimensions. However, the method as presented so far, has one possible drawback which was alluded to earlier - to obtain the Jacobi matrix we must analytically differentiate the relevant equations and boundary conditions. In this chapter we propose a procedure which will allow for the calculation of the Jacobi matrix by the use of differential approximations. The goal is to obtain the Jacobi matrix, and hence be able to calculate a range of solutions in parameter space, using the results obtained from solving the nonlinear system (I.1) at only two distinct values of $\underline{\epsilon}$. This differential approach will be applied to the case of two dimensional supersonic flow considered in Chapter 1 and to two dimensional subsonic potential flow.

In the Introduction we said that if $\underline{u}^0 = \underline{u}(\underline{x}\ ;\ \underline{\epsilon}_0)$ represented a known solution of the base flow then any neighboring flow at some fixed point $\underline{x}$ is approximated by

$$\underline{u}(\underline{x};\underline{\epsilon}) \approx \underline{u}^0 + \frac{\partial \underline{u}^0}{\partial \underline{\epsilon}_k} \quad (\underline{\epsilon}_k - \underline{\epsilon}_0) \tag{3.1}$$

The obvious first order approximation for $\dfrac{\partial \underline{u}^0}{\partial \underline{\epsilon}_k}$ is

$$\left.\frac{\partial \underline{u}^0}{\partial \underline{\epsilon}_k}\right|_{\underline{x},\ \text{fixed}} \approx \left.\frac{\underline{u}(\underline{x};\underline{\epsilon}) - \underline{u}^0}{\underline{\epsilon}_k - \underline{\epsilon}_0}\right|_{\underline{x},\ \text{fixed}} \tag{3.2}$$

What this says is that to compute $\dfrac{\partial \underline{u}^0}{\partial \underline{\epsilon}_k}$ we can take the value of $\underline{u}$ at the location $\underline{x}$ in the base flow and subtract it from the value of $\underline{u}$ found from the perturbed flow ($\underline{\epsilon} = \underline{\epsilon}_0 + \Delta\underline{\epsilon}$) *at the same location.* In practice, this may require interpolation on one computational grid.

This approach requires special attention at a boundary. In our approach both material boundaries and possible shocks are taken to be boundaries and both give rise

to locations which change with $\underline{\epsilon}$. This would certainly be the case if we chose to vary the parameters of a body.

To be more specific, we would like to be able to use the calculation of pressure in the base flow in order to compute the pressure on the new body. Thus the formulas (1.25), (1.26) are no longer applicable since they apply at a fixed field point. Therefore, to correct (1.26) we must include changes in location of the body due to changes in $\underline{\epsilon}$. In the interests of simplicity we specify a three dimensional body by

$$y = f(x,z;\underline{\epsilon}) \tag{3.3}$$

A typical quantity, say pressure, at the new body, which we will specify by $\underline{X}_0$, is related to the old body $\underline{x}_0$ in the following way

$$p(\underline{X}_0;\underline{\epsilon}) \approx p(\underline{x}_0;\underline{\epsilon}_0) + \frac{\partial p(x_0;\underline{\epsilon}_0)}{\partial \underline{\epsilon}_k} \cdot \Delta\underline{\epsilon}_k + \frac{\partial p(x_0;\underline{\epsilon}_0)}{\partial y_0} \frac{\partial f}{\partial \epsilon_k} \Delta\epsilon_k \tag{3.4}$$

where $\Delta\underline{\epsilon} = \underline{\epsilon} - \underline{\epsilon}_0$ and

$$\underline{x}_0 = (x_0, f(x_0,z_0;\underline{\epsilon}_0), z_0) \tag{3.5}$$

and

$$\underline{X}_0 = (x_0, f(x_0,z_0;\underline{\epsilon}), z_0) \tag{3.6}$$

Compare (3.4) with equation (1.26).

Note that we have related $\underline{X}_0$ to $\underline{x}_0$ by placing $\underline{X}_0$ directly above $\underline{x}_0$ in the x-z plane. Other choices are possible and may be more appropriate in certain cases.

Equation (3.4) in fact gives us the ability to compute the pressure at the new body, but requires knowledge of the differential coefficients $\frac{\partial p}{\partial \underline{\epsilon}}$. They can be obtained from

$$\frac{\partial p(\underline{x}_0;\underline{\epsilon}_0)}{\partial \underline{\epsilon}_k} \approx \frac{p(\underline{X}_0;\underline{\epsilon}) - p(\underline{x}_0;\underline{\epsilon}_0) - \frac{\partial p(\underline{x}_0;\underline{\epsilon}_0)}{\partial y_0} \frac{\partial f}{\partial \underline{\epsilon}_k} \Delta\underline{\epsilon}_k}{\Delta\underline{\epsilon}_k} \tag{3.7}$$

to first order, or

$$\frac{\partial p(x_0;\underline{\epsilon}_0)}{\partial \epsilon_k} \approx \frac{p(\underline{X}_0;(\underline{\epsilon} + \epsilon_0)/2) - p(\underline{x}_0; \frac{3\underline{\epsilon}_0}{2} - \frac{\underline{\epsilon}}{2}) - \frac{\partial p(x_0; \frac{3\underline{\epsilon}_0}{2} - \frac{\underline{\epsilon}}{2})}{\partial y_0} \frac{\partial f}{} \Delta\underline{\epsilon}_k}{\Delta\underline{\epsilon}_k} \tag{3.8}$$

It should be noted that the differential determination of the differential coefficient $\frac{\partial p}{\partial \underline{\epsilon}}$ requires not only calculation of the different flow fields, but also of $\frac{\partial p}{\partial y_0}$. Therefore, in the numerical calculation it is necessary to compute $\frac{\partial p}{\partial y_0}$ at the body. This we do by interpolation.

To illustrate these remarks we return to the case treated in Chapter 1. We consider two dimensional supersonic flow at thicknesses of 10% and 10.1% to calculate $\frac{dx}{d\epsilon}$, $\frac{dy}{d\epsilon}$, $\frac{d\theta}{d\epsilon}$, $\frac{d\mu}{d\epsilon}$, $\frac{ds}{d\epsilon}$. Using equation (3.8) the resulting derivatives were then used to compute the pressue distribution on a 15% thick airfoil (Figure 1). Note that this pressure distributuion compares favorably with that computed from using the Jacobi matrix generated by solving the differential equations (Chapter 1, Figure 3). The error between the two computations is less then 1%.

2D SUBSONIC FLOW

As a second illustration we apply the Jacobi matrix technique to the potential equation for two dimensional compressible flow. The potential equation is derived by assuming inviscid, irrotational flow and is valid for subsonic flows and for low transonic flows when boundary layer effects can be neglected.

Since we have implemented the Jacobi technique by modifying Jameson's computer code FLO36 we will summarize the derivation of the relevant equations and their solution [1],[2].

Under the assumption of irrotational flow we may introduce a velocity potential ϕ such that

$$u = \phi_x \qquad v = \phi_y \tag{3.9}$$

The potential satisfies the quasilinear equation

$$(a^2 - u^2)\ \phi_{xx} - 2uv\ \phi_{xy} + (a^2 - v^2)\ \phi_{yy} = 0 \tag{3.10}$$

where a is the local speed of sound. When given the ratio of specific heats γ, the stagnation speed of sound a_0 and the local speed $q = \sqrt{u^2 + v^2}$ the speed of sound is determined by

$$a^2 = a_0^2 - \frac{\gamma - 1}{2}\ q^2 \tag{3.11}$$

We will consider (3.10) for subsonic flows. (But see Figure 9 for a transonic case).

At the body the flow must satisfy the tangentcy conditionn

$$\frac{\partial \phi}{\partial n} = 0 \tag{3.12}$$

where n is the normal derivative and the Kutta condition - that the tangential velocity is bounded at the trailing edge. In the far field the potential approaches the potential of a vortex in compressible flow and a uniform stream. The density and pressure are determined by relations

$$p^{\gamma - 1} = M_\infty^2\, a^2 \tag{3.13}$$

and

$$p = \frac{p^\gamma}{\gamma M_\infty^2} \tag{3.14}$$

The coordinate system used for computation is generated by conformally mapping the exterior of the airfoil to the interior of the unit circle. The airfoil itself becomes the coordinate line r = 1 (Figure 2).

Since the far field boundary condition must now be applied at r = 0, where the

potential becomes infinite, a reduced potential which removes this singularity is introduced by

$$G = \phi - \frac{\cos(\theta+\alpha)}{r} + E(\theta+\alpha) \tag{3.15}$$

Here α is the angle of attack and $2\pi E$ is the circulation.

If the modulus of the transformation from the physical plane to the circle plane is denoted by H then (3.10) becomes

$$(a^2 - u^2)G_{\theta\theta} - 2uvrG_{r\theta} + (a^2 - v^2)r\frac{\partial}{\partial r}(rG)$$

$$- 2uv(G_\theta - E) + (u^2 - v^2)rG_r + (u^2 + v^2)\left(\frac{u}{r}H_\theta + vH_r\right) = 0 \tag{3.16}$$

The u and v are the velocity components in the θ and r directions, respectively and are given by

$$u = \frac{r(G_\theta - E) - \sin(\theta+\alpha)}{H}, \quad v = \frac{r^2 G_r - \cos(\theta+\alpha)}{H} \tag{3.17}$$

The Neumann boundary condition (3.12) becomes

$$G = \cos(\theta+\alpha) \quad \text{at } r = 1 \tag{3.18}$$

while the far field condition is

$$G = E\{\theta + \alpha - \tan^{-1}[\sqrt{1 - M_\infty^2}\tan(\theta+\alpha)]\} \text{ at } r = 0 \tag{3.19}$$

The circulation is determined by the Kutta condition which requires that the velocity be finite at the trailing edge of the airfoil. Here we have $H = 0$ and $\phi_\theta = 0$ so (3.15) reduces to

$$E = G_\theta - \sin\alpha \quad \text{at} \quad r = 1, \ \theta = 0 \tag{3.20}$$

The details of the calculation of H and of the multigrid solution of (3.16)-3.20)

are not essential for our purposes and are discussed in references [1], [3], [4], [5]. The important point is that the transformation to the circle plane is conformal so that every airfoil in the physical plane is mapped to a circle and every physical flow is mapped to the interior of the circle.

CALCULATION OF THE JACOBI MATRIX

The equations for computing the Jacobi matrix by finite differences were given by equations (3.4)-(3.8). In the subsonic case the only parameter changed was the airfoil thickness based on chord. Due to the construction of equation (3.16) the quantities which are of interest are the reduced potential G, and the metric H. To define the locations $\underline{x}$ in equation (3.2) we note that in the circle plane the points are spaced angularly (θ) as 2π/(the number of grid points about airfoil) and radially (r) as 1/(the number of grid points from airfoil to far field). Therefore, it is natural to define the location $\underline{x}$ by the intersection of these lines.

The variational flow was computed using essentially the same procedure which was used to calculate the pressure in the two dimensional supersonic flow case. In the transformed plane we first compute the flow about an airfoil of thickness ϵ_1 and save the converged values of G and H. Next we compute the flow about an airfoil of thickness ϵ_0. We use these computed values of G and H along with those from the run at thickness ϵ_1 to compute $\frac{dG}{d\epsilon}$ and $\frac{dH}{d\epsilon}$ using (3.7). G and H for the variational flow at thickness ϵ is computed using equation (3.4).

RESULTS

Figure 3 shows the results of a parametric calculation using a base airfoil of 10% thickness based on chord and a second airfoil of 10.1% thickness to predict the pressure distribution on a 14% thick airfoil. It should be noted that there is very close agreement between the parametric calculation and the solution given by FLO36.

Figure 4 uses a 10% thick airfoil and 10.1% thick airfoil to calculate the flow

over 15% thick profile - that is, a profile which is 50% more than the base airfoil. Again the agreement is quite good. Figures 5 through 8 show the same calculations for flows at different Mach numbers. All show close agreement between the parametrically generated solutions and those given by FLO36.

The method breaks down when there is a drastic change in the behavior of the solution in the parameter space. This is illustrated in Figure 9. Here the flows about the 10% and 10.1% thick airfoils are subsonic but the flow about the 15% thick airfoil is supercritical. The method is unable to account for the shock.

FIGURE CAPTIONS

Fig. 1. Pressure distribution on 10% and 15% thick airfoils at M = 4 calculated by direct differencing along with respective bodies.

Fig. 2. Computational plane, from [2].

Fig. 3. Pressure distribution on 14% thick airfoil, M = 0.75. Solid curve is FLO36 result, dashed is parametric. Base and new airfoils are also shown.

Fig. 4. Pressure distribution on 15% thick airfoil, M = 0.75. Solid curve is FLO36 result, dashed is parametric. Base and new airfoils are also shown.

Fig. 5. Pressure distribution on 14% thick airfoil, M = 0.60. Solid curve is FLO36 result, dashed is parametric. Base and new airfoils are also shown.

Fig. 6. Pressure distribution on 15% thich airfoil, M = 0.60. Solid curve if FLO36 result, dashed is parametric. Base and new airfoils are also shown.

Fig. 7. Pressure distribution on 14% thick airfoil, M = 0.45. Solid curve is FLO36 result, dashed is parametric. Base and new airfoils are also shown.

Fig. 8. Pressure distribution on 15% thick airfoil, M = 0.45. Solic curve is FLO36 result, dashed is parametric. Base and new airfoils are also shown.

Fig. 9. Pressure distribution on 15% thick airfoil, M = 0.80. Solid curve is FLO36 results, dashed is parametric. Base and new airfoils are also shown.

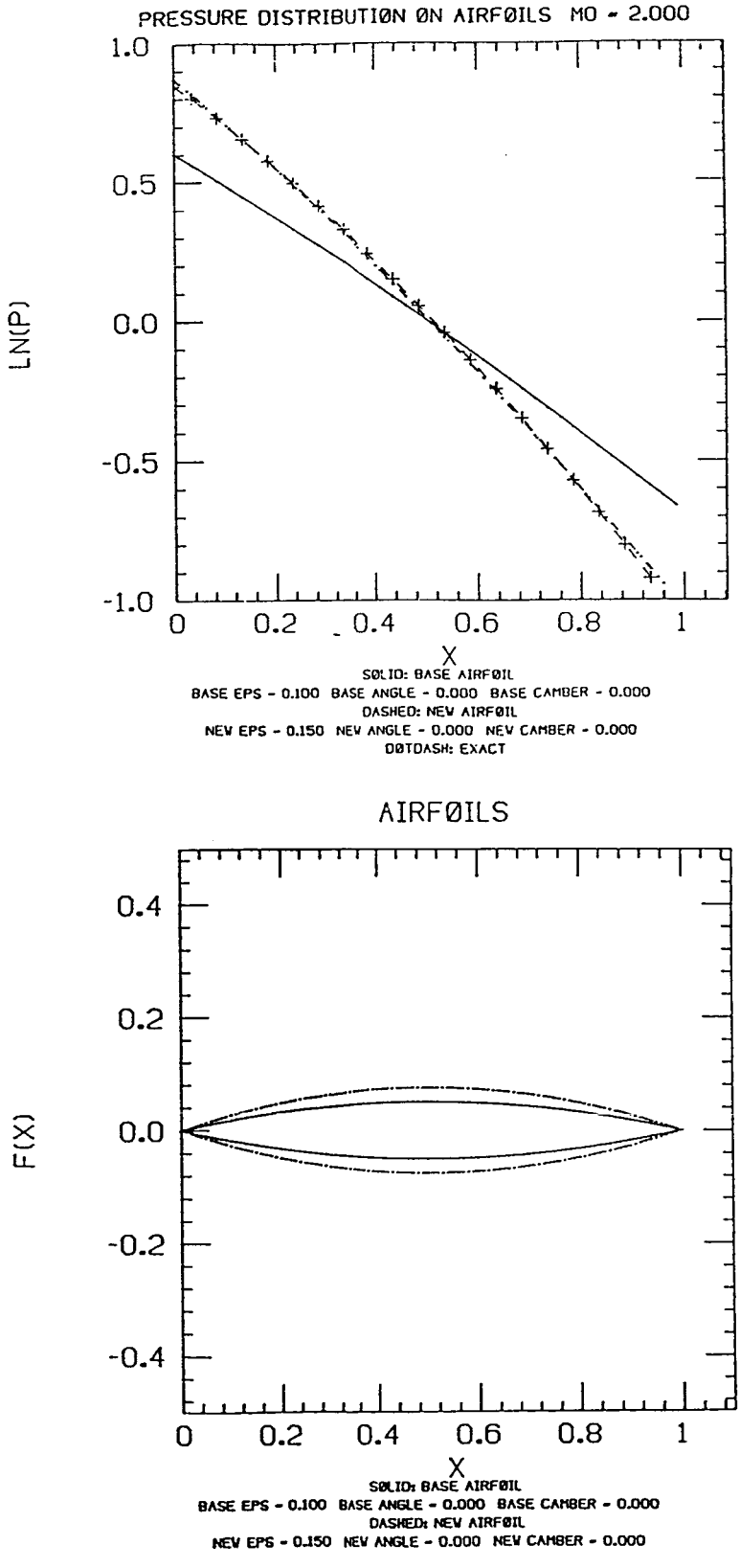
PRESSURE DISTRIBUTIØN ØN AIRFØILS MO = 2.000
LN(P)
1.0
0.5
0.0
-0.5
-1.0
0
0.2
0.4
0.6
0.8
1
X
SØLID: BASE AIRFØIL
BASE EPS = 0.100 BASE ANGLE = 0.000 BASE CAMBER = 0.000
DASHED: NEW AIRFØIL
NEW EPS = 0.150 NEW ANGLE = 0.000 NEW CAMBER = 0.000
DØTDASH: EXACT
AIRFØILS
F(X)
0.4
0.2
0.0
-0.2
-0.4
0
0.2
0.4
0.6
0.8
1
X
SØLID: BASE AIRFØIL
BASE EPS = 0.100 BASE ANGLE = 0.000 BASE CAMBER = 0.000
DASHED: NEW AIRFØIL
NEW EPS = 0.150 NEW ANGLE = 0.000 NEW CAMBER = 0.000

Figure 1

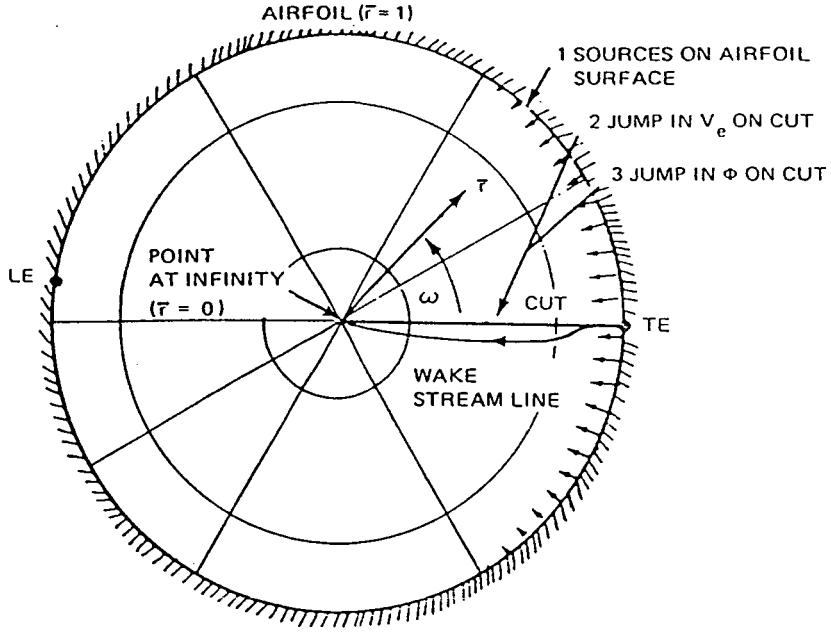
AIRFOIL ($\bar{r}$ = 1)
1 SOURCES ON AIRFOIL SURFACE
2 JUMP IN V_e ON CUT
3 JUMP IN Φ ON CUT
LE
POINT AT INFINITY ($\bar{r}$ = 0)
$\bar{r}$
ω
CUT
TE
WAKE STREAM LINE

Figure 2

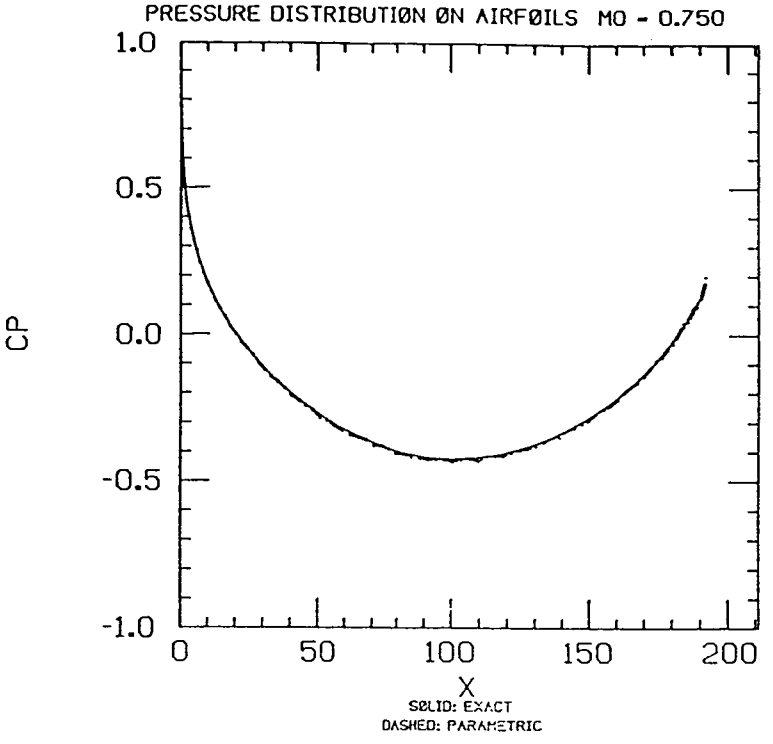
PRESSURE DISTRIBUTIØN ØN AIRFØILS MO - 0.750
1.0
0.5
0.0
-0.5
-1.0
CP
0
50
100
150
200
X
SØLID: EXACT
DASHED: PARAMETRIC

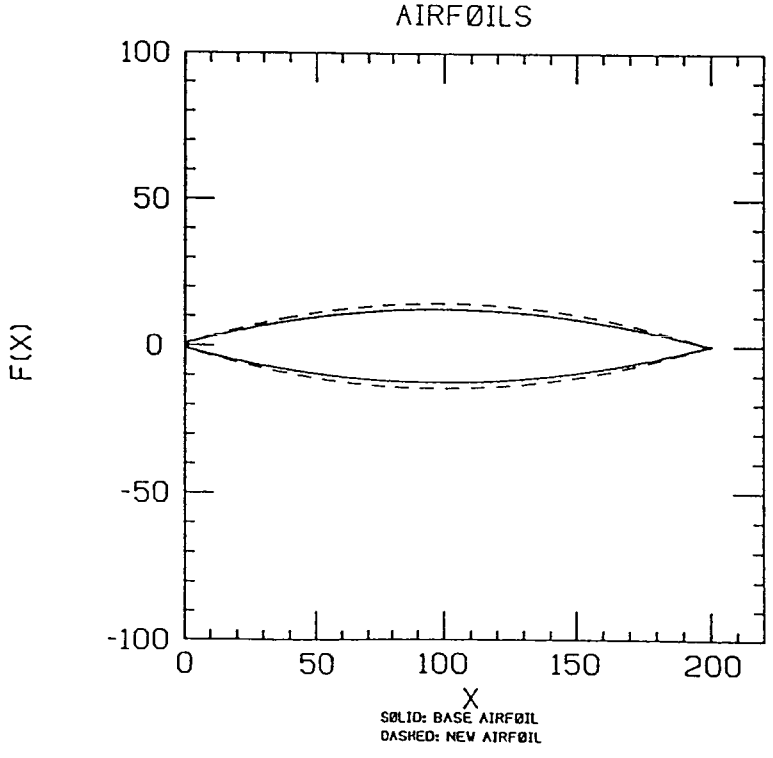
AIRFØILS
100
50
0
-50
-100
F(X)
0
50
100
150
200
X
SØLID: BASE AIRFØIL
DASHED: NEW AIRFØIL

Figure 3

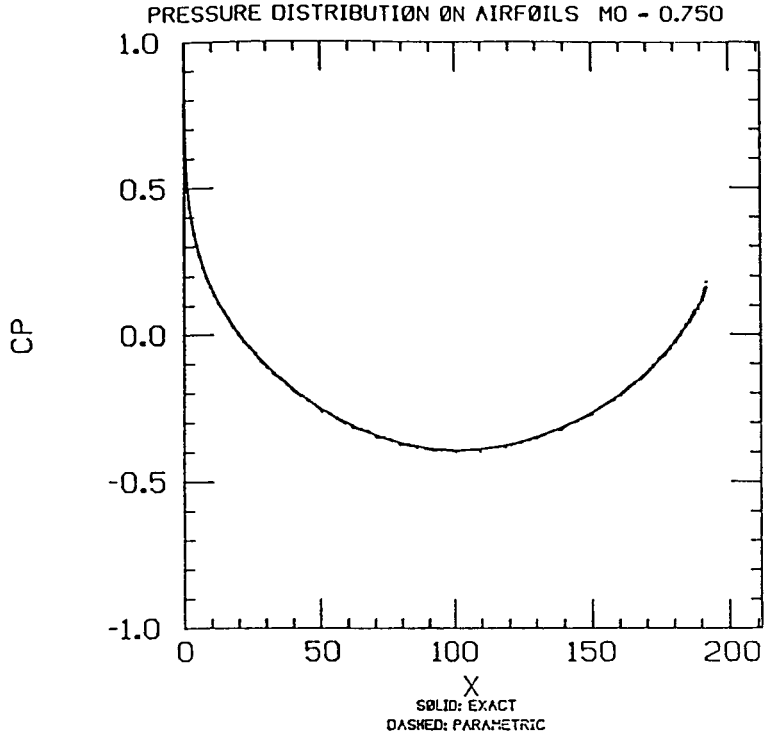
PRESSURE DISTRIBUTIØN ØN AIRFØILS MO - 0.750
1.0
0.5
0.0
-0.5
-1.0
CP
0
50
100
150
200
X
SØLID: EXACT
DASHED: PARAMETRIC

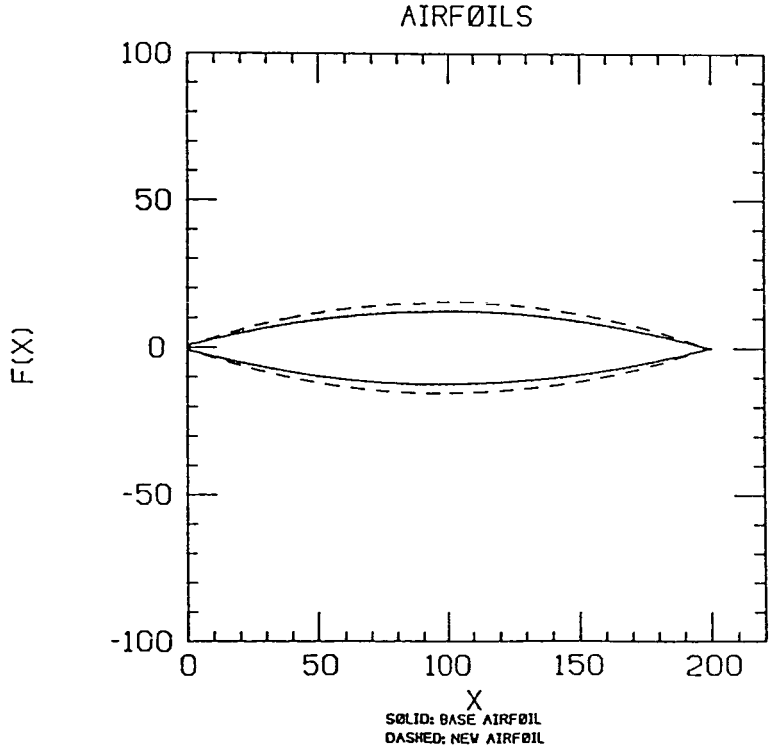
AIRFØILS
100
50
0
-50
-100
F(X)
0
50
100
150
200
X
SØLID: BASE AIRFØIL
DASHED: NEW AIRFØIL

Figure 4

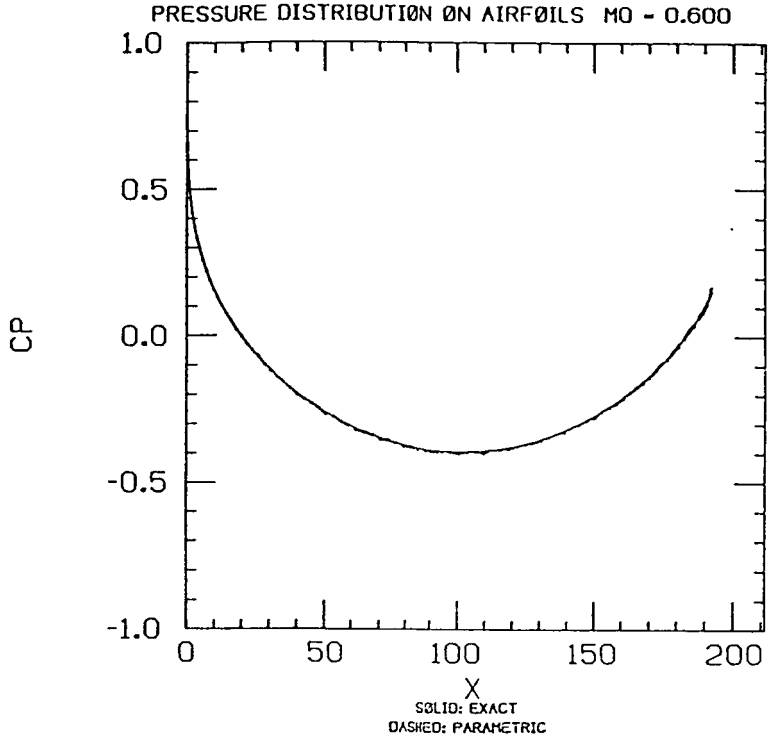
PRESSURE DISTRIBUTIØN ØN AIRFØILS MO - 0.600
1.0
0.5
0.0
-0.5
-1.0
CP
0
50
100
150
200
X
SØLID: EXACT
DASHED: PARAMETRIC

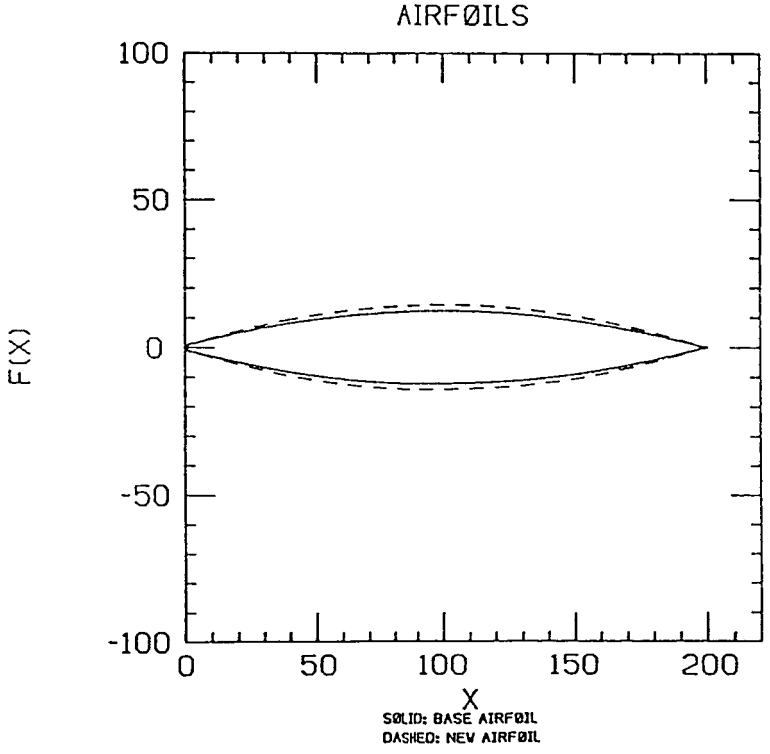
AIRFØILS
100
50
0
-50
-100
F(X)
0
50
100
150
200
X
SØLID: BASE AIRFØIL
DASHED: NEW AIRFØIL

Figure 5

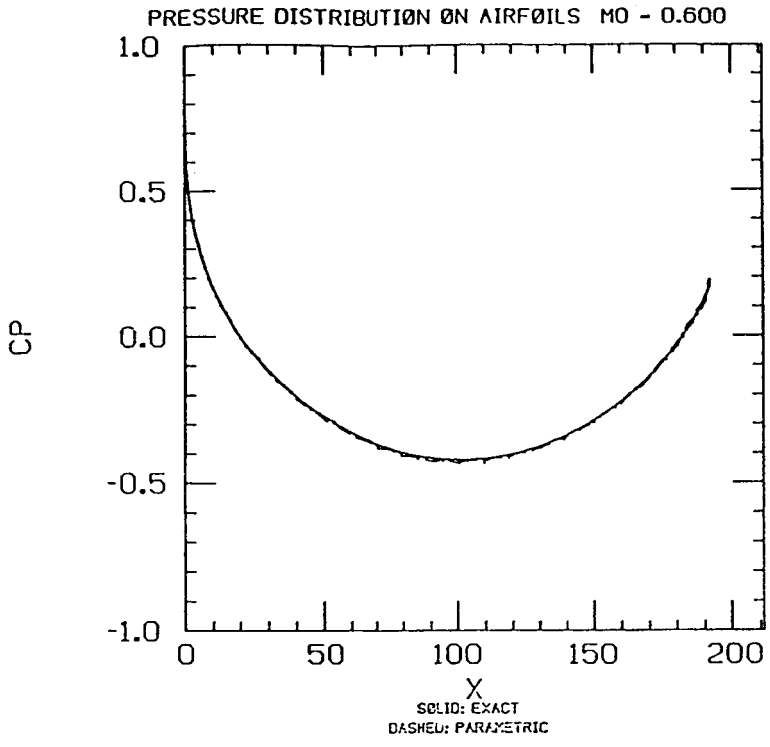
PRESSURE DISTRIBUTIØN ØN AIRFØILS MO - 0.600
1.0
0.5
0.0
-0.5
-1.0
CP
0
50
100
150
200
X
SØLID: EXACT
DASHED: PARAMETRIC

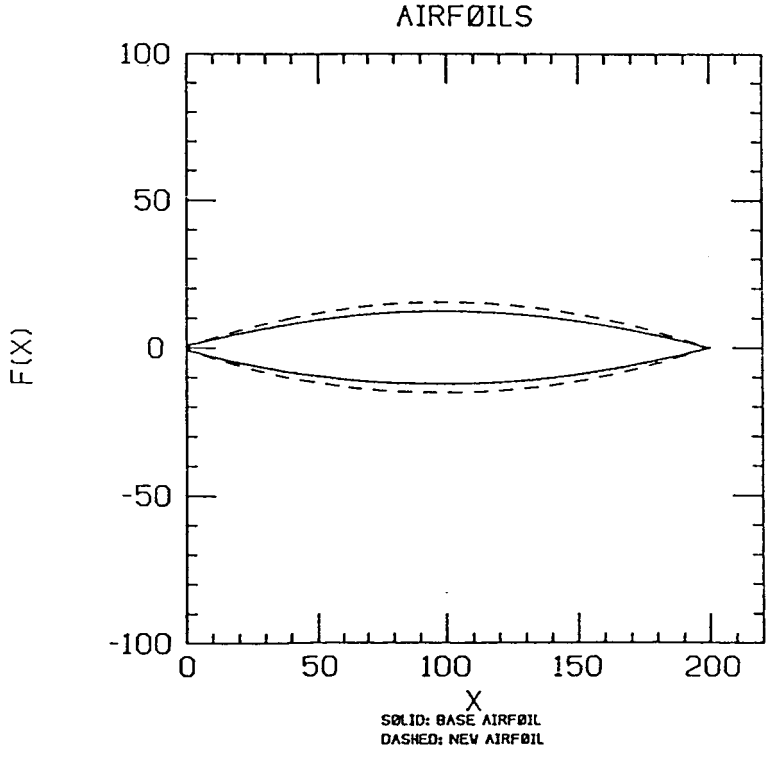
AIRFØILS
100
50
0
-50
-100
F(X)
0
50
100
150
200
X
SØLID: BASE AIRFØIL
DASHED: NEW AIRFØIL

Figure 6

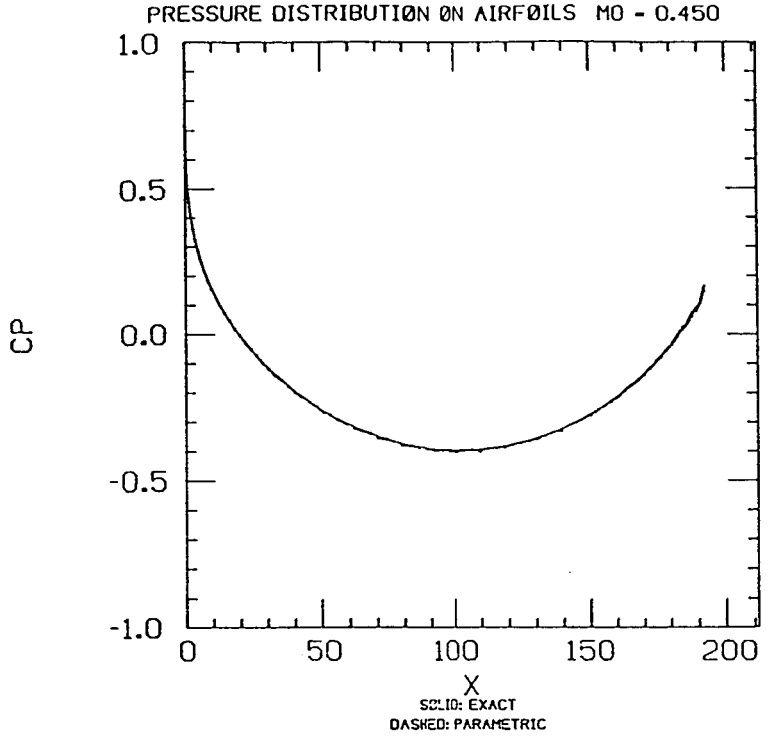
PRESSURE DISTRIBUTIØN ØN AIRFØILS MO - 0.450
1.0
0.5
0.0
-0.5
-1.0
CP
0
50
100
150
200
X
SØLID: EXACT
DASHED: PARAMETRIC

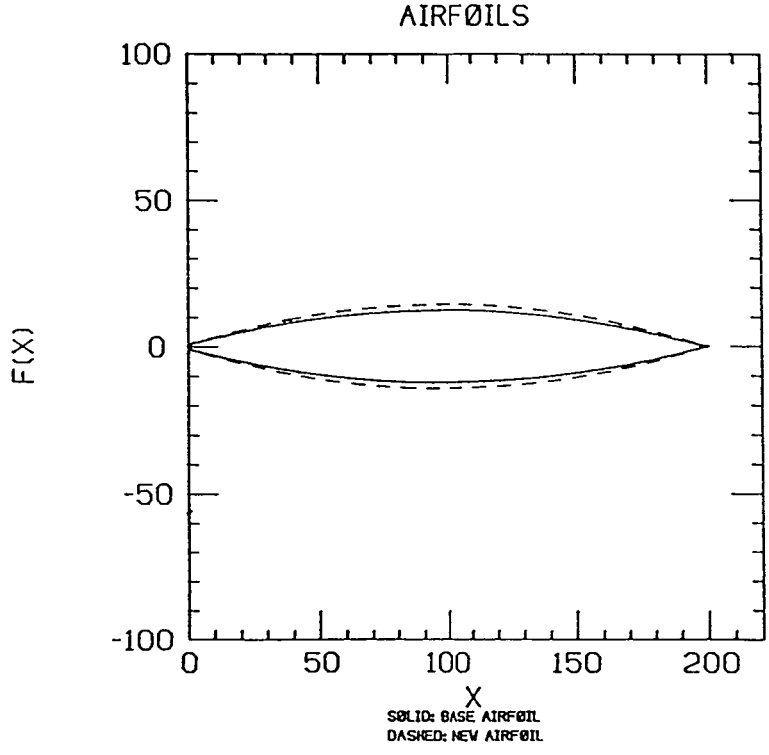
AIRFØILS
100
50
0
-50
-100
F(X)
0
50
100
150
200
X
SØLID: BASE AIRFØIL
DASHED: NEW AIRFØIL

Figure 7

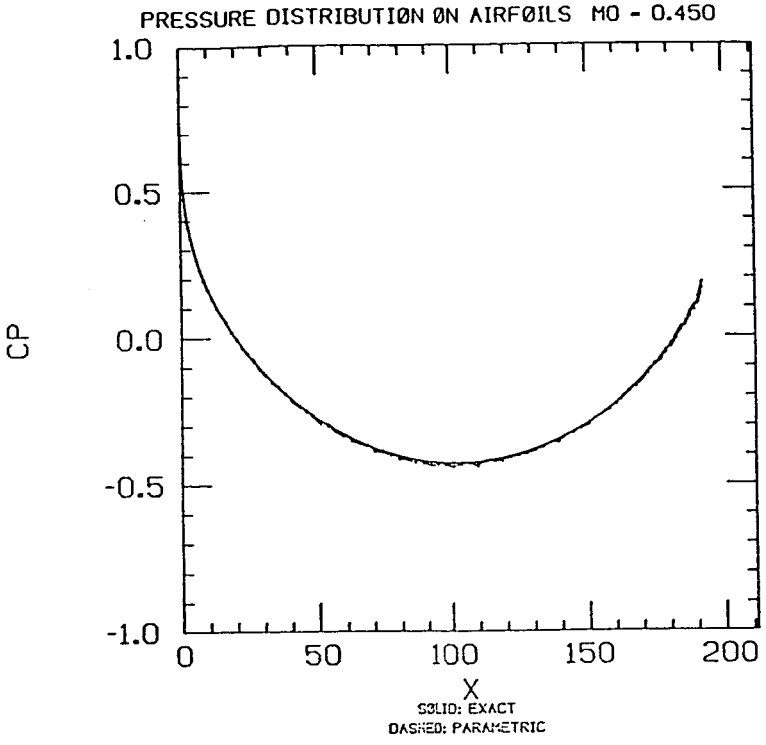
PRESSURE DISTRIBUTIØN ØN AIRFØILS MO - 0.450
CP
1.0
0.5
0.0
-0.5
-1.0
0
50
100
150
200
X
SØLID: EXACT
DASHED: PARAMETRIC

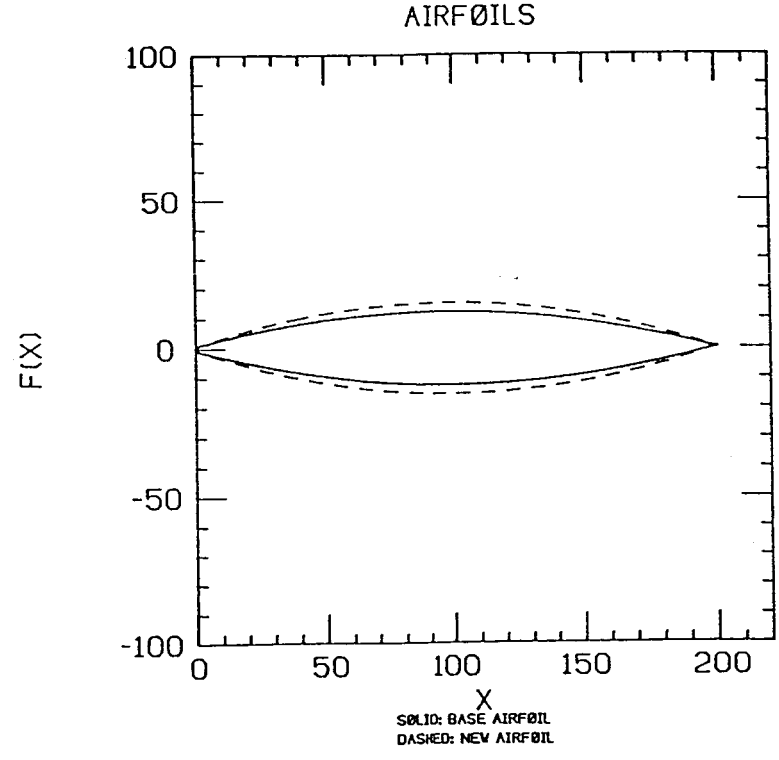
AIRFØILS
F(X)
100
50
0
-50
-100
0
50
100
150
200
X
SØLID: BASE AIRFØIL
DASHED: NEW AIRFØIL

Figure 8

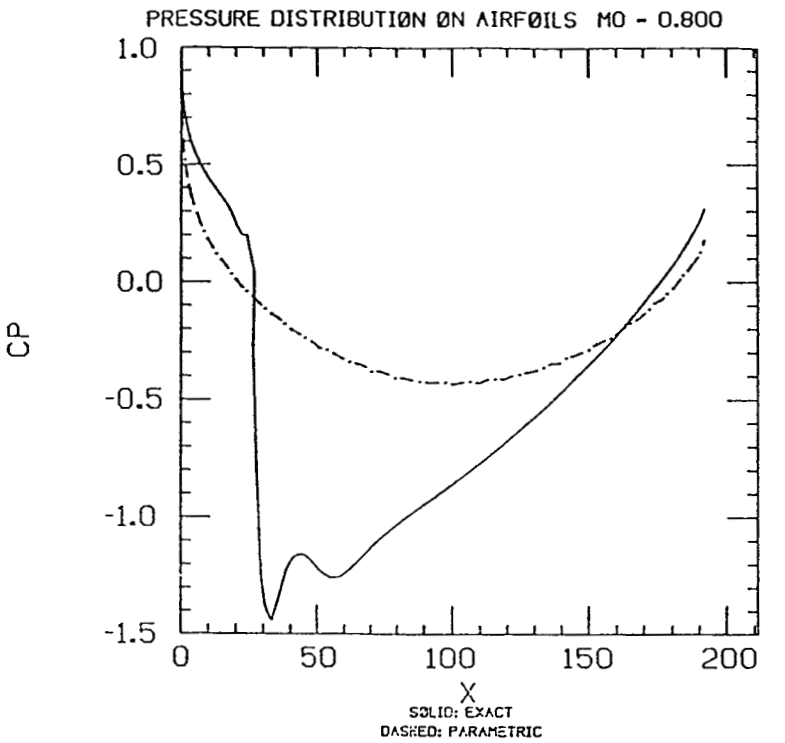
PRESSURE DISTRIBUTIØN ØN AIRFØILS MO - 0.800
1.0
0.5
0.0
-0.5
-1.0
-1.5
CP
0
50
100
150
200
X
SØLID: EXACT
DASHED: PARAMETRIC

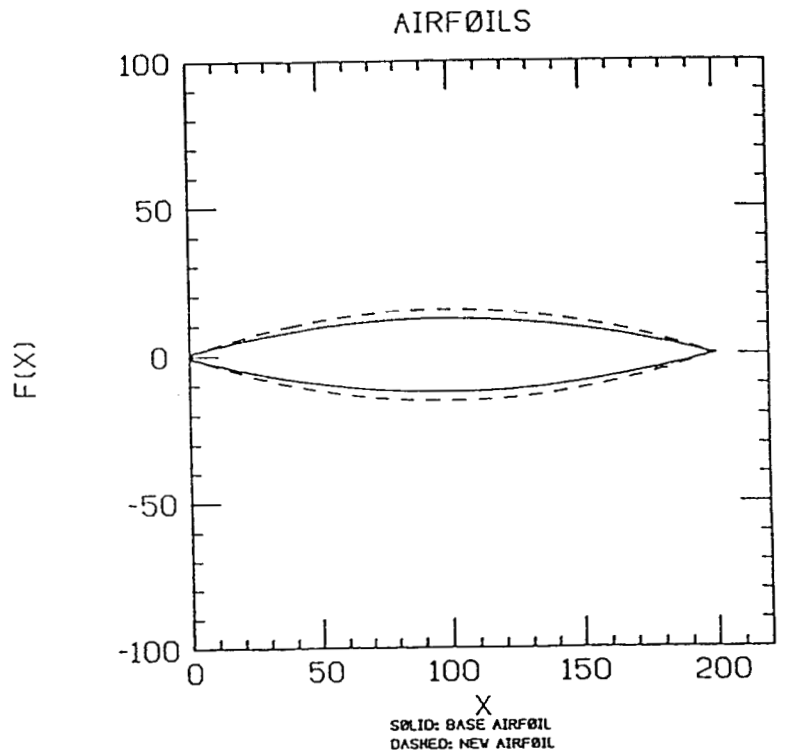
AIRFØILS
100
50
0
-50
-100
F(X)
0
50
100
150
200
X
SØLID: BASE AIRFØIL
DASHED: NEW AIRFØIL

Figure 9

REFERENCES

[1] Jameson, Antony, **"Acceleration of Transonic Potential Flow Calculations on Arbitrary Meshes by the Multiple Grid Method"**, AIAA 79-1458

[2] Melnik, R.E., Chow, R.R., Mead, H.R., Jameson, A., **"An Improved Viscid/Inviscid for Transonic Flow Over Airfoils"**, NASA CR-3805, 1985.

[3] Jameson, Antony, **"Transonic Flow Calculations"** in Wirz, H.J. and J.J. Smolderen (ed), Numerical Methods in Fluid Dynamics, McGraw-Hill Book Co., 1978.

[4] Bauer, F., Garabedian, P., Korn, D., Jameson, A., **"Supercritial Wing Section II"**, Springer-Verlag, New York, 1975.

[5] Jameson, Antony, **"Transonic Flow Calculations"**, Lecture Notes, Courant Institute of Mathematical Sciences, New York, 1976.

[6] Jameson, Antony, **"The Evolution of Computational Methods in Aerodynamics"**, MAE Report No. 1608, May 1983.